UNIVERSITY OF CALIFORNIA, SAN DIEGO

Quest for a Turnover Mechanism in Peptide-Based Enzyme Mimics

A dissertation submitted in partial satisfaction of

the requirements for the degree

Doctor of Philosophy

in

Engineering Sciences (Mechanical Engineering)

by

Tsukasa Takahashi

Committee in charge:

Professor Michael J. Heller, Chair
Professor Gaurav Arya
Professor Joanna M. McKittrick
Professor Frank E. Talke
Professor Andrea R. Tao

2015

The Dissertation of Tsukasa Takahashi is approved, and it is acceptable in quality and form for publication on microfilm and electronically;

_____

_____

_____

_____

_____

Chair

University of California, San Diego

2015

Dedication

To my family and friends for their love and support.

Epigraph

Desiderata

Max Ehrmann

Table of Contents

List of Figures

List of Tables

Acknowledgements

I would like to thank Professor Michael Heller for his support as the chair of my committee. It has been an honor to be a part of his goal to achieve truly synthetic enzyme mimics.

I would also like to acknowledge Michelle Cheung who spent the most time with me in the lab to move this project forward. Thomas Butterweck and Steve Schankweiler both deserve mention as well for their hours spent discussing and running experiments throughout their undergraduate career. Bao Vo Ngo and Alive Xiao also deserve credit for their excellent work done on the molecular dynamics simulation and Professor Gaurav Arya for allowing me to collaborate with them. Finally, I would like to thank Amy Pan for continuing the project in the future.

Other lab members have helped me through these years, namely: Avery Sonnenberg, Youngjun Song, and Jennifer Wright. All have provided me tremendous amount of insight, technique, and knowledge.

I would like to thank Dr. Ed Sheldon and Lynn Foster for their effort to move the technology forward by starting Z-Field Technologies and working on the patent and grant writing process.

Chapters 2, in part, has been published in Catalysis Communications, “Quest for a turnover mechanism in peptide-based enzyme mimics,” by T. Takahashi, M. Cheung, T. Butterweck, S. Schankweiler, and M. J. Heller (2015) **59**, 206-210, and has been submitted for publication in Biochemistry, “Molecular mechanical properties of short sequence peptide enzyme mimics” by T. Takahashi, B. C. Ngo, L. Xiao, G. Arya, and M. J. Heller (2015). The dissertation author is the primary investigator in these publications.

Vita

2009	Bachelor of Science, University of California, San Diego
2009-2011	Teaching Assistant, Department of Mechanical Engineering University of California, San Diego
2011	Master of Science, University of California, San Diego
2009-2014	Graduate Student Researcher, University of California, San Diego
2012-2015	Teaching Assistant, Department of Nanoengineering University of California, San Diego
2015	Doctor of Philosophy, University of California, San Diego

Publications

"Quest for a turnover mechanism in peptide-based enzyme mimics" Catalysis Communication Volume 59, pp206-210, January 2015

"Molecular mechanical properties of short sequence peptide enzyme mimics" Biochemistry February 2015

Fields of Study

Major Field: Mechanical Engineering

Studies in Mechanical Biomimetic Material Science

Abstract of the Dissertation

Molecular Mechanical Properties of Short Sequence Peptide Enzyme Mimics

by

Tsukasa Takahashi

Doctor of Philosophy in Engineering Sciences (Mechanical Engineering)

University of California, San Diego, 2015

Professor Michael J. Heller, Chair

Creation of synthetic structures with an enzyme-like mechanism and turnover remains a significant challenge. In this study, peptides containing a cysteine thiol and histidine imidazole group were designed to mimic the active site of the cysteine protease papain. Ellman's reagent trapping experiments showed that rapid acetyl group exchange exists between the thiol and imidazole groups. This exchange rate increased significantly in peptides with bulky R-groups (phenylalanine) between the cysteine and histidine. A

reduction of the cysteine thiol pKa and NMR results further support closer proximity of the thiol and imidazole groups in peptides with faster acetyl group exchange. We have also used NAMD and VMD simulation to determine the distance between these catalytic groups and the overall mechanical flexibility of the peptides. We found important correlations between the Cys-His distance deviation, which determines the flexibility between the two molecules, and its relationship to the deacylation rate. We found that generally, shorter Cys-His distance deviations allow for a higher deacylation rate constant, meaning that greater confinement of the two residues will allow a higher frequency of the acetyl exchange between the cysteine thiol and histidine imidazole R-groups. This may be the key to future design of peptide structures with molecular mechanical properties that lead to viable enzyme mimics. End of this study include our initial attempts in stabilizing the peptides with the use of nanoparticles, micelles, and functionalized surfaces. We have also shown our initial concept which utilizes electric field in order to control the negatively charged cysteine thiol and the positively charged histidine imidazole to achieve a truly mechanically controlled molecular system to produce catalytic effects. Although much work needs to be done, our preliminary results show promise in the growth of new techniques that can be built upon in the future.

1

Introduction

1.1 Enzyme Mimetics

Of all the macromolecules in living organisms, enzymes represent those that are the most complicated in terms of mechanistic properties. Enzymes are able to catalyze the transformation of all other biomolecules, providing the dynamics and very essence of life. In this era of nanotechnology, enzymes can aptly be considered bio-nanomachines that do chemistry. These bio-nanomachines catalyze reactions with high specificity and enormous rate accelerations; some producing millions of turnovers per second.

Over the last several decades, considerable efforts have been made to create synthetic versions of enzymes, which are sometimes called synzymes, chemzymes, or nanozymes(1-4). Although, some progress has been made with enzyme mimics, most attempts have failed, and the few successes exhibit only marginally catalytic properties. A few examples include supramolecular structures (e.g. cyclodextrins), polypeptides, metal complexes, and nanoparticles and nanostructures, which have become of more

interest in the past decade(5-18). Computational models have become a basis for understanding and designing chemical structures that mimic enzymes as well as for optimizing existing enzymes for specific reactions. Increasingly popular method combining the known structures of the enzyme and computational modeling techniques are the evolutionary approach to improve the existing enzyme. In short, directed evolution is a method in which existing proteins or structures are allowed to mutate through natural evolutionary processes while being screened for improvements in one or more properties(19-24). Despite these efforts in enzyme mimics, only mild success has been recorded even in the most recent studies.

1.2 Cysteine Protease Mechanism

When creating an enzyme, the most direct approach is to mimic the amino acid structure of the enzyme. Although exact amino acid sequence and the protein structures of existing enzymes are known, recreating the secondary, tertiary, and quaternary structure is virtually impossible mainly due to the completely different environment the synthetic enzymes are created. Instead of recreating the entire amino acid structure, the common approach taken is the use of the critical amino acids used in the enzyme. The main site that is responsible for enzyme proteolytic activity is known as the catalytic triad. Its ubiquitous occurrences in many enzymes emphasize the importance of this structural motif and side group interactions. In particular, the catalytic triad of the cysteine protease papain consists of Cys-25, His-159, and Asp-175, while serine protease chymotrypsin contains Ser-195, His-57, and Asp-102. Figure 1 shows papain and its catalytic triad. Figure 2 shows the mechanism of chymotrypsin which consists of its catalytic site

creating a pocket and cleaving the substrate in a machine-like manner. The nature of these enzymes' three dimensional structure and mechanical movement are attributed to the precise location of their catalytic groups. In their native condition during catalysis, the imidazole of histidine is neutral, and the thiol or hydroxyl group initiates the reaction by launching a nucleophilic attack on the substrate. Histidine, being zwitterionic, accepts a proton from the nucleophile, forming an intermediate complex, and then transfers the bound substrate away, restoring the enzyme to its original state. Although there have been several mechanisms proposed for this process, the cooperating triad structure has remained consistent(25-36).

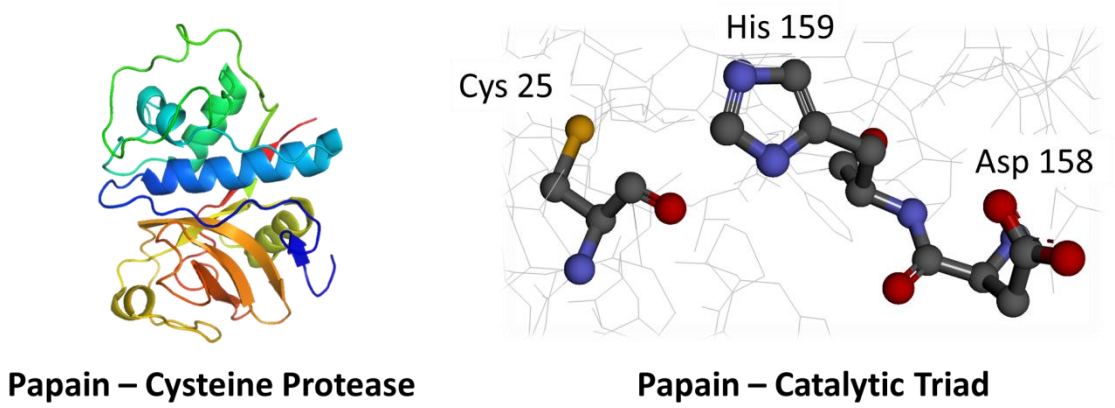

Figure 1: Structure of papain (left) and its catalytic sites (right).

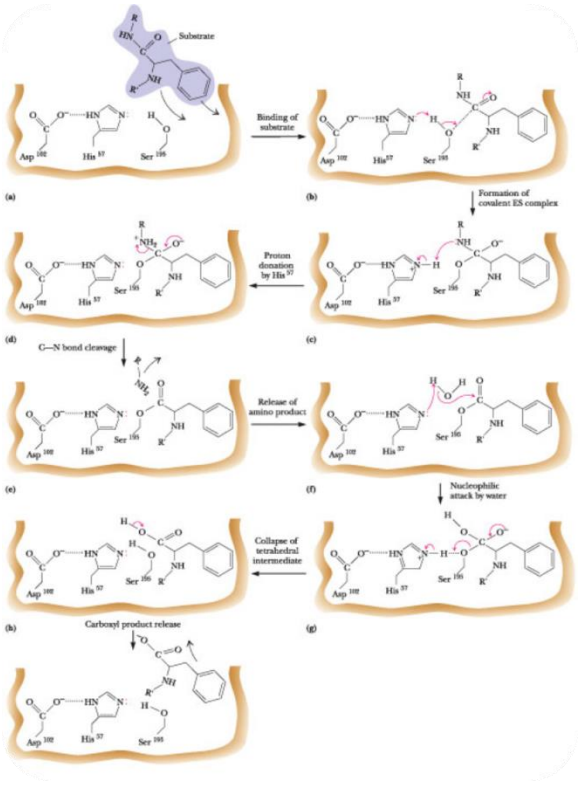

Figure 2: Chymotrypsin mechanism.

1.3 Studies on enzyme mimics using amino acid structures

In early work on synzymes, Heller et al. designed and synthesized cysteine and histidine peptides that were intended to mimic the catalytic site of papain(30). While no significant turnover was observed, there was evidence that a reversible intramolecular transfer of the acetyl group was occurring between the cysteine thiol and histidine imidazole groups, where the equilibria favor the acetyl-thiol intermediate as shown in Figure 4. Such results suggest that if the back-attack by the cysteine thiol could be prevented, subsequent hydrolysis of the acyl-imidazole intermediate would produce a leaving group mechanism that leads to turnover. This is because the acetyl-imidazole intermediate is more than two orders of magnitude more labile to hydrolysis than the

acetyl-thiol intermediate. While the formation of a covalent acyl-imidazole intermediate is not believed to be part of the actual papain or chymotrypsin reaction mechanisms, enzymes do overcome similar back-attack reactions and do exhibit distinct mechanical movements. Indeed, evidence exists for major dynamic movement of the histidine imidazole group in chymotrypsin catalysis(28, 29). More recently, Kisailus et al. designed and synthesized nanostructures as mimics for the catalytic site of the hydrolase enzyme silicatein, which has a serine and histidine at its active site. In this work, aliphatic hydroxyl and imidazole groups were placed in parallel arrangements on a gold surface as shown in Figure 3. The interface between chemically distinct monolayers provided juxtaposition of nucleophilic (hydroxyl) and hydrogen-bonding (imidazole) groups. Such arrangements should have the potential to catalyze the hydrolysis of a gallium oxide precursor, and template the condensed product formation of gallium oxohydroxide (GaOOH) and gamma-gallium oxide (-Ga_2O3)(12).

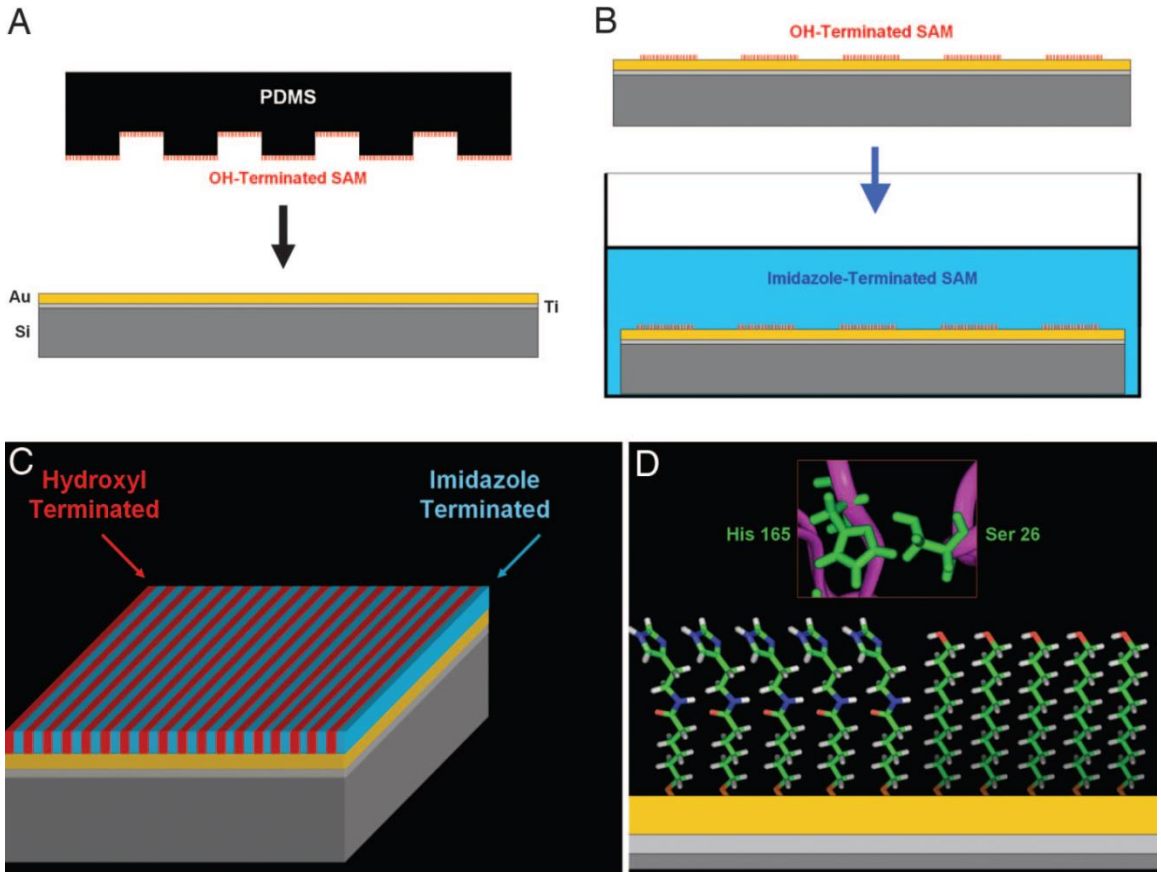

Figure 3: Schematic of the self-assembled monolayer done by Morse et. al.(12)

While this study demonstrates a form of template-based heterogeneous catalysis, which is different from homogeneous ester and amide hydrolysis, it again shows the importance of the imidazole group in performing hydrolysis reactions. The study also demonstrates a new role that nanotechnology may ultimately play in the development of viable synthetic catalysts. Several other enzyme-like nanostructures derived from short-sequence peptides have now also been studied that show further promise for peptide-based catalysts(37). The goal of our study was to further investigate the acetylation and deacylation mechanism in new peptide constructs where the cysteine thiol and histidine imidazole groups are in close proximity. The peptides also contained aspartate, which provided a

carboxyl group in the vicinity of the histidine imidazole. A better understanding of the dynamics of these catalytic groups in the acyl exchange mechanism is of key importance to the further development of viable synzymes which can produce turnover.

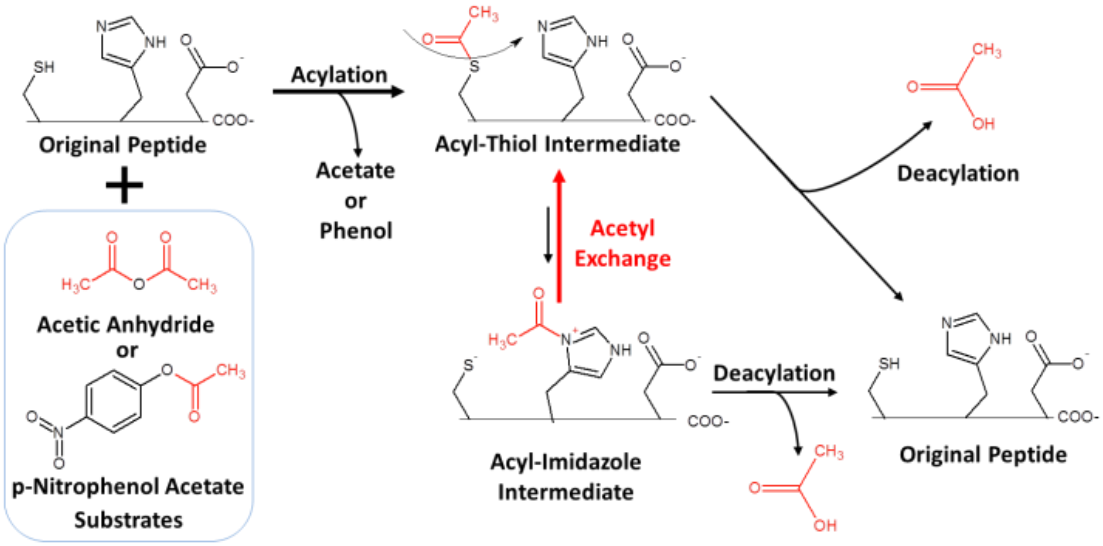

Figure 4: Scheme showing the peptide acetylation and deacylation process. The quick acetyl group exchange between the thiol and imidazole prevents turnover(30, 37)(30, 37).

After the initial acylation of the substrates, acyl-thiol and acyl-imidazole intermediates exchange the acetyl group. This prevents the final deacylation step to occur. Our goal is to design and test synthetic enzymes that begin to mimic the acetylation and deacylation mechanism of the cysteine proteases by using short-sequence peptides that contain the main entities of the protease reaction site. In addition, we have incorporated initial studies using nanoparticles, nano-structures, and surfaces that allow us to control the catalytic groups with higher precision.

1.4 Techniques in this study

The enzyme activity was measured by reacting the substrate with the enzyme and measuring the hydrolysis rate of the substrate. The substrates can hydrolyze on their own

at certain pH, temperature, or ionic content in the buffer. All substrates have different rate of hydrolysis due to their molecular nature. For example, p-nitrophenol acetate was often used since they have a very fast and controlled rate of hydrolysis that can be measured simply by taking measurements on the UV-Vis spectrophotometer. These substrate reactions are measured over time in a UV-Vis spectrophotometer or a fluorometer depending on their activity upon hydrolysis.

Adding peptides with the catalytic groups to these substrates is the simplest form of catalysis. In general, there are two basic modes of peptide-substrate catalysis. Homogeneous catalysis requires the catalytic molecules to be suspended in solution. Heterogeneous catalysis requires the catalytic molecules to be attached to a surface. We will be looking at both cases in our study. Especially for the electric field studies, the requirement of heterogeneous structures becomes critical due to the directional nature of electric field.

Largely, we have two methods of studying our enzyme: acetylation and deacylation. The former allows us to measure the actual turnover rate of the enzyme since it requires that the enzymes return to its original form in order for them to produce repeated acetylation reactions. The latter, deacylation rate is often measured in our studies to characterize the transfer rate of the acetyl group from the thiol to the imidazole group. Although the acetyl transfer rate is not exactly synonymous as the deacylation rate, they are numerically close since blocking of the thiol group with the Ellman's Reagent allows the deacylation to occur once the acyl-imidazole forms.

2

Homogeneous Peptide Catalysis

In this chapter, peptides were tested in a homogeneous solution where they reacted freely with the substrates. They were tested without any further conjugation or attachment to any surface.

1.1 Methods

1.1.1 Peptides Studied

Listed in Table 1 are the nine peptides used in this study (95% purity verified by HPLC from Genscript). The peptides were combinations of cysteine (sulfhydryl/thiol), serine (hydroxyl), histidine (imidazole) and aspartate (carboxyl), along with seven other amino acids which included alanine, phenylalanine, glycine, arginine, lysine, asparagine, and proline. Peptide 1 consisted of a cysteine and serine but excludes the histidine, which leads to the loss of the acetyl-transfer effect. Peptide 2 contains a cysteine, histidine and aspartate, and produces some acetyl group transfer. Peptides 3 and 4 are variations of Peptides 1 and 2, respectively, with an arginine at the c-terminus introducing a positively

charged group. Peptides 5 and 6 are further variations of Peptide 4, with phenylalanines adjacent to cysteine to provide a bending of the peptide backbone structure to produce a closer proximity of cysteine thiol and histidine imidazole groups (Figure). Peptide 7 has the cysteine and histidine in reverse order and examines the effects of arginine on aspartate. Peptide 8 acts as a control for Peptide 7 by replacing the histidine with asparagine, which lacks reactivity for acetyl group exchange. Peptide 9 is composed of fourteen amino acids, and incorporates two extra histidines and a proline that produces further bending of the backbone (Figure 5). All nine peptides have their n-terminus acetylated in order to avoid nonspecific nucleophilic reaction by the α-amino group.

Peptides 14, 16, and 18 vary by the addition of Phe and Gly-Phe between Lys-Cys, respectively. Peptides 15, 17, and 19 are the equivalents of Peptides 14, 16, and 18 with the addition of Gly-Asp at the c-terminus. These enzymes were designed to find the effects of chain length and the addition of aspartate next to the histidine on the c-terminus. Figure 5 shows Peptides 14 through 19 with color-coded cysteine and histidine. Peptides 2, 4, 5, 6, 7, 9, and 14 through 19 were also used for the molecular dynamic simulation.

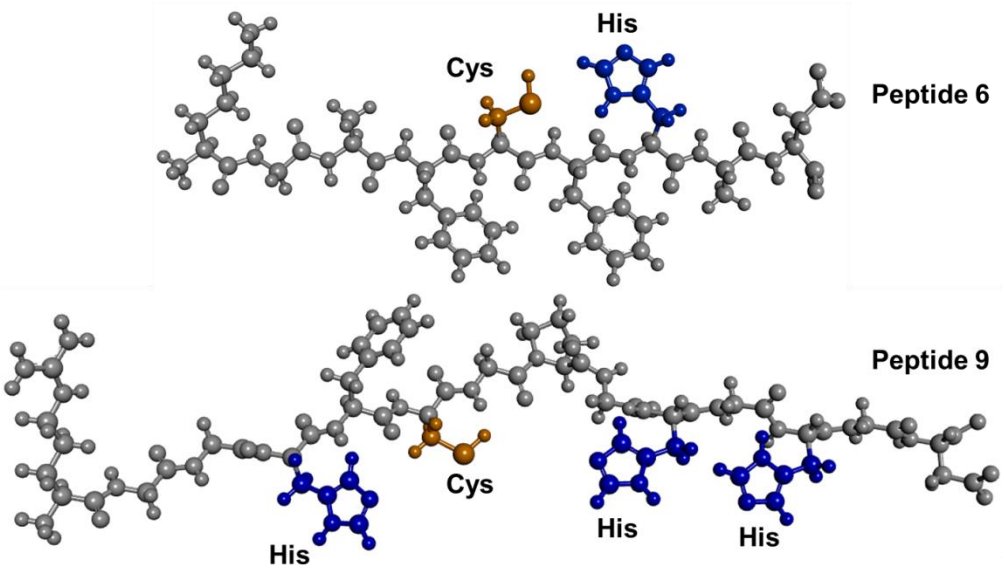

Figure 5: Peptides 6 and 9 with cysteine and histidines labeled in orange and blue respectively.

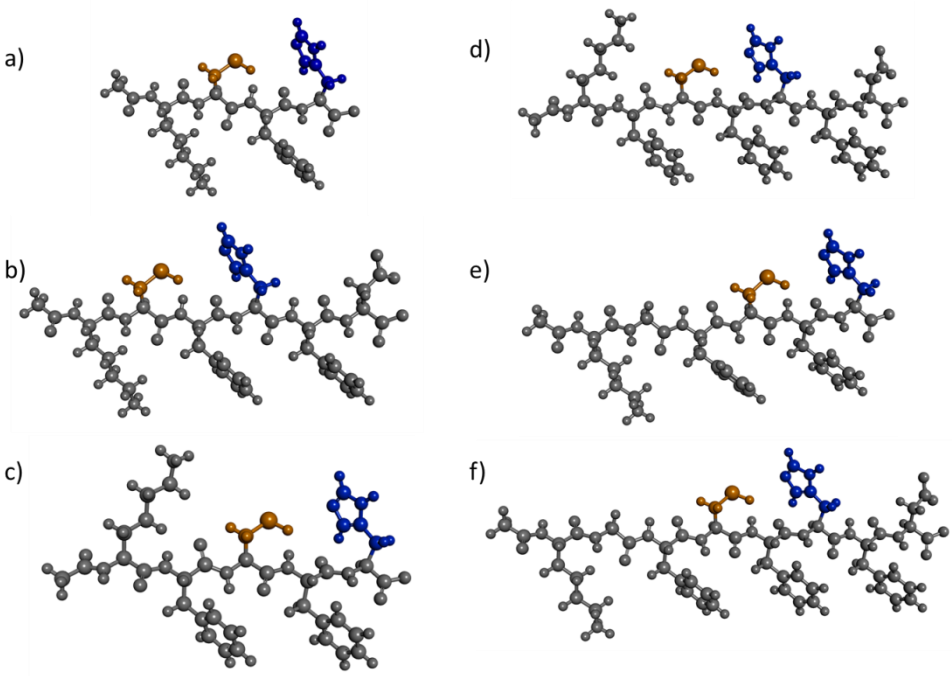

Figure 6: Peptides a) 14, b) 15, c) 16, d) 17 e) 18, f) 19 with cysteine and histidine labelled in orange and blue respectively.

Table 1: List of Controls and Peptides 1 through 19.

Name	Compound/Sequence
Control 1	p-Nitrophenyl acetate (pNPA)
Control 2	Acetic Anhydride (AA)
Control 3	n-Acetyl l-Cysteine
Control 4	n-Acetyl l-Histidine
Control 5	n-Acetyl l-Cysteine + n-Acetyl l-Histidine
Control 6	n-Acetyl l-Cysteine + n-Acetyl l-Histidine + n-Acetyl l-Lysine (ACAHAL)
Peptide 1	Ac-Gly-Gly-Ala-Ala-Cys-Ala-Ser-Ala-Asp
Peptide 2	Ac-Gly-Gly-Ala-Ala-Cys-Ala-His-Ala-Asp
Peptide 3	Ac-Arg-Gly-Ala-Ala-Cys-Ala-Ser-Ala-Asp
Peptide 4	Ac-Arg-Gly-Ala-Ala-Cys-Ala-His-Ala-Asp
Peptide 5	Ac-Arg-Gly-Ala-Phe-Cys-Phe-His-Ala-Asp
Peptide 6	Ac-Lys-Gly-Ala-Phe-Cys-Phe-His-Ala-Asp
Peptide 7	Ac-Arg-Asp-Phe-His-Phe-Cys-Ala-Gly-Asp
Peptide 8	Ac-Arg-Asp-Phe-Asn-Phe-Cys-Ala-Gly-Asp
Peptide 9	Ac-Arg-Gly-Gly-His-Phe-Cys-Gly-Pro-Gly-His-Gly-His-Gly-Asp
Peptide 14	Ac-Lys-Cys-Phe-His
Peptide 15	Ac-Lys-Cys-Phe-His-Phe-Asp
Peptide 16	Ac-Lys-Phe-Cys-Phe-His
Peptide 17	Ac-Lys-Phe-Cys-Phe-His-Phe-Asp
Peptide 18	Ac-Lys-Gly-Phe-Cys-Phe-His
Peptide 19	Ac-Lys-Gly-Phe-Cys-Phe-His-Phe-Asp

Each of the peptides was reacted with the substrate p-nitrophenyl acetate (pNPA) or acetylated by acetic anhydride and the corresponding acylation/deacylation rate constants were calculated.

1.1.2 **Acetylation**

Peptides 14 through 19 were initially diluted to approximately 10 mM in DI water. The concentrations of the peptides were checked by measuring the total amount of cysteine using the Ellman's Reagent and comparing the 10 mM n-acetyl l-cysteine absorbance values at 412 nm. The substrate p-nitrophenyl acetate (pNPA) was diluted in ethanol, also to 10 mM. Each peptide was further diluted in 0.1 M Tris-Borate (TB)

buffer, pH 8.5, and then the pNPA was added to start the reaction. The reaction was carried out at 20 °C for 30 minutes. The reaction concentration for both peptide and substrate was 100 µM in a final volume of 600 µL. The peptide reaction rates were determined along with Controls 1 and 2 – each substrate for acetylation and deacylation alone, Control 3 – 100 µM of n-acetyl l-cysteine (AC), Controls 4 – n-acetyl l-histidine (AH), Control 5 – Combination of Controls 3 and 4, and Control 6 – Control 5 with the addition of n-acetyl l-lysine (AL). The absorbance of the cleaved p-nitrophenol was measured at 400 nm with a Perkin Elmer UV-Vis Lambda 800 during the 20-minute reaction time. The reaction scheme is shown in Figure 7. The second-order rate constants for the acetylation process were determined from the initial rates according to the equation:

$$k_a = \frac{initial\ rate - spontaneous\ rate}{[catalyst][substrate]}$$

where the spontaneous rate is the hydrolysis rate of pNPA.

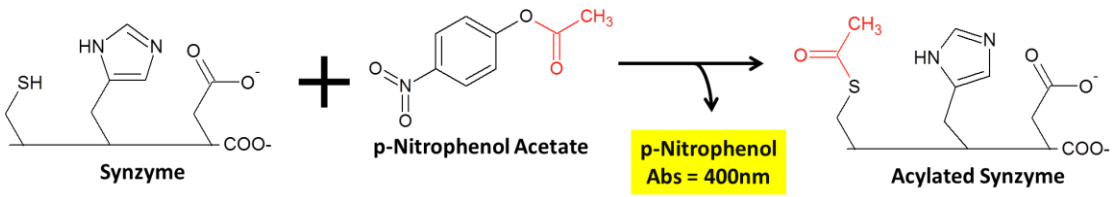

Figure 7: Scheme of acetylation rate experiment using p-nitrophenol acetate.

For Peptides 6, 18 and 19, additional acetylation experiments were performed at five pH values in 0.1x TB buffer and four times the original substrate concentration of 2 mM. This test was performed in order to see the effect of the imidazole changing on the pKa of the neighboring cysteine thiol. The cysteine thiol (pKa = 8.14) is normally 10%

deprotonated at pH 7.2; 25% at pH 7.74; 50% at pH 8.14; 75% at pH 8.67, and 90% at pH 9.13.

1.1.3 **Deacylation & Ellman's Reagent Trapping**

All peptides and controls were acetylated with a 15-fold excess of acetic anhydride (AA) injected as a 10% by volume solution in acetonitrile. The acetylation of the imidazole and the thiol groups of the peptides was observed for 20 minutes at 270 nm and 235 nm, respectively, to ensure the completion of the reaction. Subsequently, deacylation by trapping was examined by adding Ellman's reagent (5,5'-dithiobis-(2-nitrobenzoic acid)) at four times the concentration of the peptides and the controls. The scheme is shown in Figure 8. Ellman's reagent irreversibly alkylates the free thiol anion when the acetyl group transfers from the thiol to the imidazole. This trapping reaction prevents back-attack by the thiol group, allowing the acetyl-imidazole group to deacylate. The deacylation of the acetyl-imidazole correlates with increase in absorbance of the cleaved Ellman's reagent (2-nitro-5-thiobenzoate) at 412 nm. A first-order rate constant for the deacylation process was determined with the initial rate according to the equation:

$$k_a = \frac{initial\ rate}{[catalyst]}$$

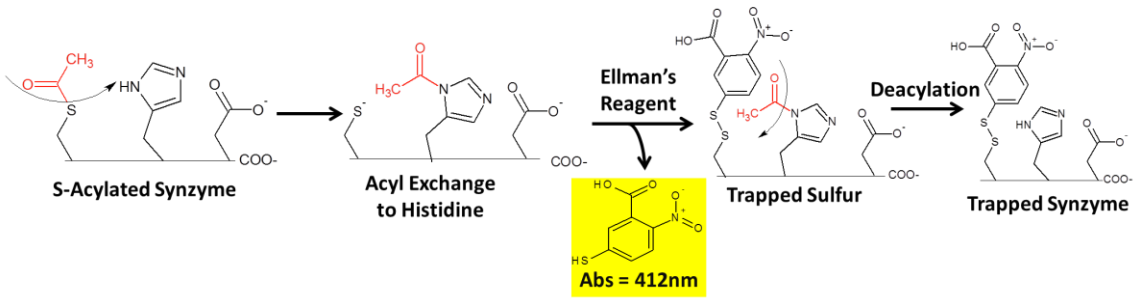

Figure 8: Scheme of deacylation rate measurement using Ellman's Reagent trapping.

1.1.4 **NMR**

1D Proton NMR spectra of Peptides 1 through 6 and controls were obtained with a Varian VX 500 NMR spectrometer provided from UCSD Department of Chemistry and Biochemistry. All spectra were recorded with 10% D_2O and 90% deionized water as solvent with a water suppression treatment. The concentration of all peptides and controls recorded in the spectrum was approximately 100 μM and prepared minutes before the experiment to minimize denaturation or oxidation. All spectra were recorded with a data size in time domain of 512 points. The water peak is suppressed from 4.5-5 ppm for better signal-to-noise ratio.

1.2 Results and Discussion

1.2.1 **Acetylation**

Between Peptides 1 through 9, all peptides but Peptide 8 showed an increase in acetylation rate compared to Control 5 (ACAH). In particular, Peptides 2, 5, 6, and 9 showed the most increase compared to Control 5 (Figure 9). While there is clearly a rate increase for these peptides, it is not exceptional. The increases are most likely due to some enhancement of the nucleophilic attack by the thiol anion ($-S^-$). As further demonstrated, in spite of the rapid acetyl group exchange that is occurring with the histidine imidazole group in Peptides 5, 6, and 9, back-attack by the thiol prevents turnover and any further rate enhancement.

Figure 10 shows the acetylation rates for pNPA, pNPA with ACAH control, and for Peptide 6 at the different pHs. For both the controls and Peptide 6, as the pH decreases, the percentage of $-S^-$ anion decreases and acetylation rate decreases. However, there is an

increase in the ratio between Peptide 6 acetylation rate and ACAH control rate as the pH decreases. This is consistent with the histidine imidazole group being situated in close proximity to the neighboring cysteine and lowering the thiol group pKa by proton abstraction (general acid-base catalysis). The effect is not seen in the ACAH control since imidazole and thiol groups are not in close proximity.

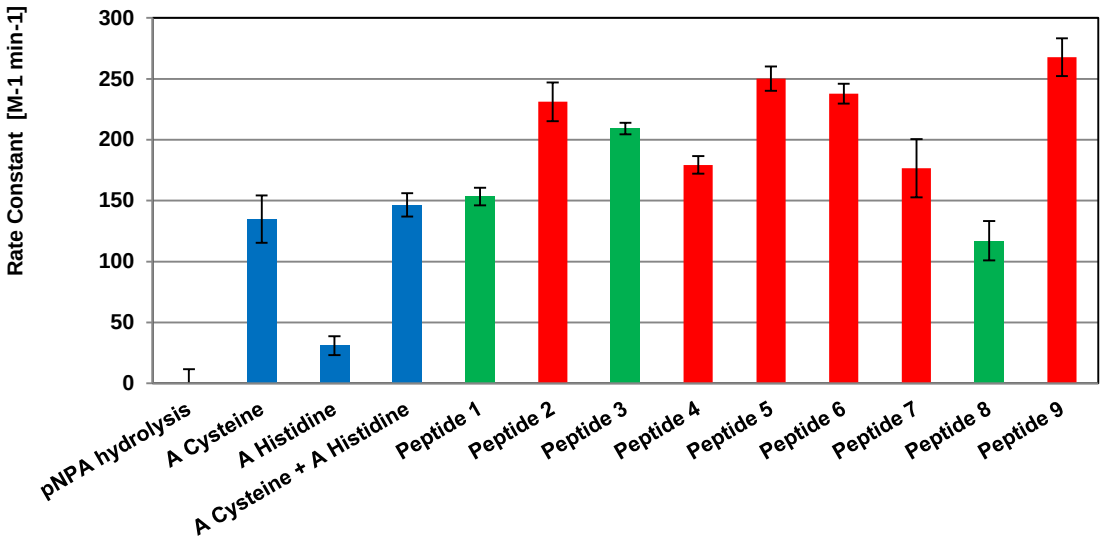

Figure 9: Acetylation rate of controls and Peptide 1 through 9.

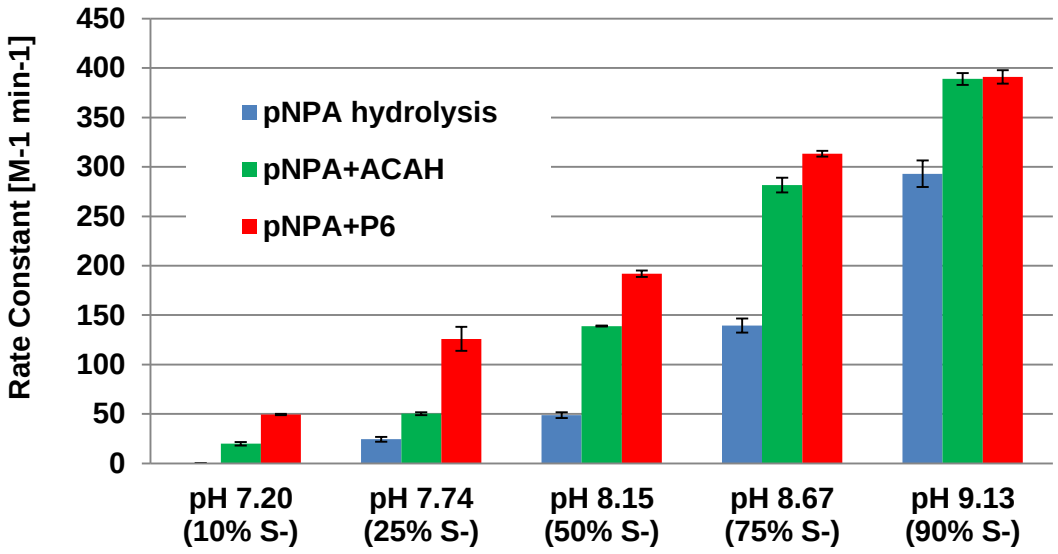

Figure 10: pNPA hydrolysis rate and acetylation rate for ACAH Control 5 and Peptide 6 at various pH values.

Acetylation rates of Peptides 14 through 19 are shown in Figure 11. Although the acetylation rates of the peptides were slightly higher than the lone amino acid control (ACAHAL), we did not see a significant increase similar to the previous sets of peptides. These increases once again are believed to be related to the increase in the nucleophilic attack by the thiol anion. The back-attack by the thiol is still present, and this prevents the effective turnover that we hope to see.

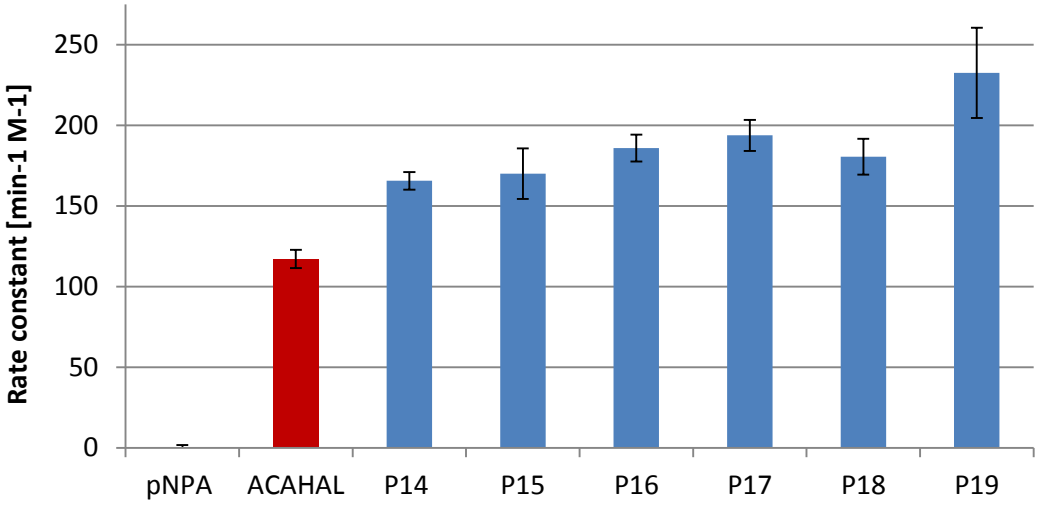

Figure 11: Acetylation rate constants of Peptide 14 through 19 and controls.

Peptides 18 and 19 were further studied to see the effect of lowering of the pH and the results are shown in Figure 12. The lowering of the pKa was previously seen in Peptide 6 and was expected in Peptides 18 and 19 as well. As the pH is lowered below the thiol pKa (pH = 8.15), the rate ratio between P18/P19 and ACAHAL increases. At pH 7.20, the deacylation rate ratio of Peptide 18/ACAHAL is 1.80 and Peptide 19/ACHAL is 1.40. Although the lowering of the thiol pKa was observed for the peptides, it is interesting to note that Peptide 19, which contains the extra Phe-Asp at the c-terminus, had no effect on further changing the pKa of the cysteine.

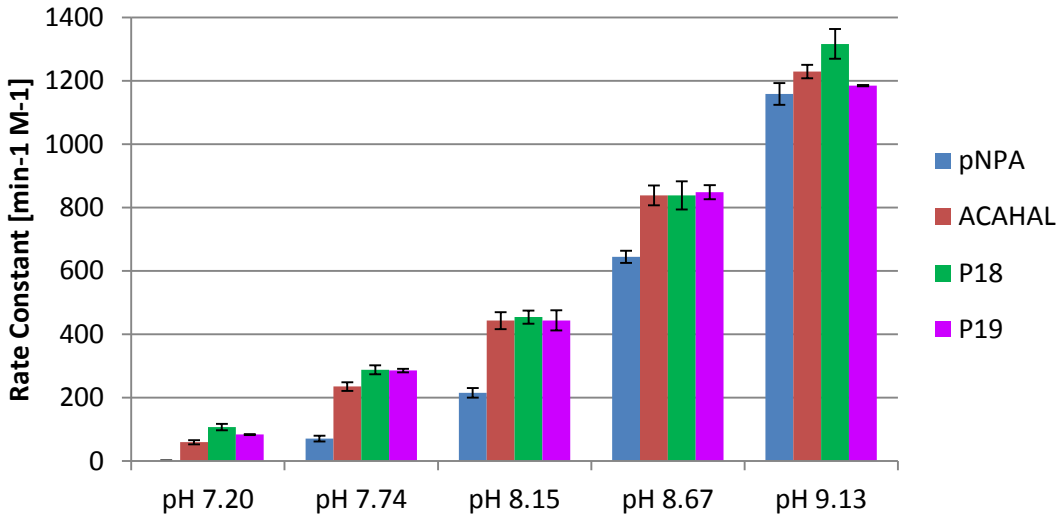

Figure 12: Acetylation rate constants of Peptides 18, 19, and controls at variable pH 7.20 (10% S-), pH 7.74 (25% S-), pH 8.15 (50% S-), pH 8.67 (75% S-), and pH9.13 (90% S-).

1.2.2 Deacylation & Ellman's Reagent Trapping

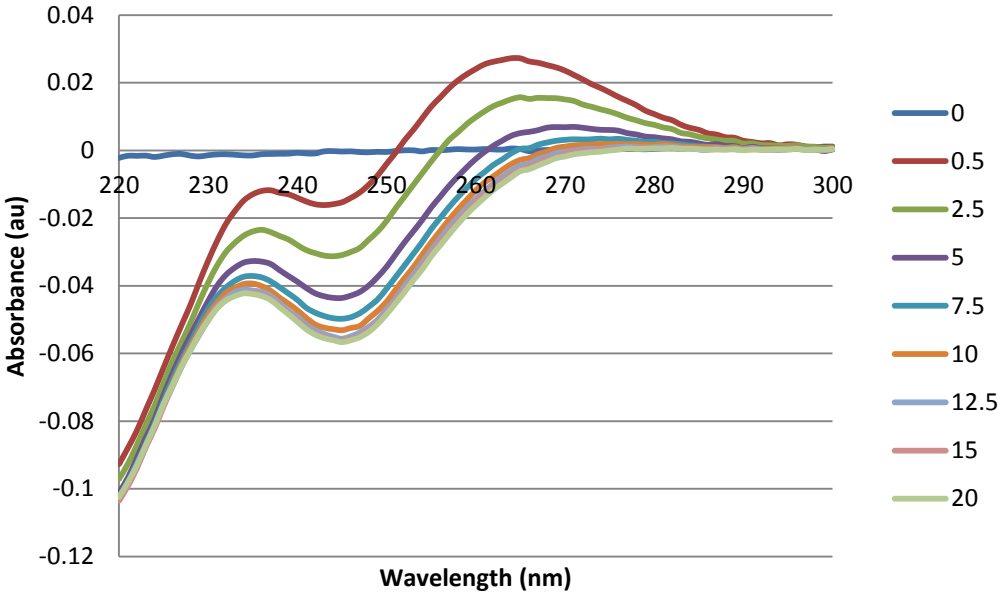

Figure 13: Acetylation rate of Peptide 6 with acetic anhydride showing peak at 235nm for acetyl-cysteine and decreasing peak of acetyl-histidine at 265nm.

Figure 13 shows the initial acetylation process using acetic anhydride. Two peaks are shown at 235nm and 270nm corresponding to the increase/decrease in concentration

of acetyl-cysteine and acetyl-histidine. The acetyl-histidine peak shows a very quick spike once inserted in the peptide solution and lowers to zero around 10 minutes. This indicates that the reaction has reaches an equilibrium and the initially acetylated histidine has all deacylated. By confirming this deacylation process, we can focus on the real issue, which is the acetyl transfer between the thiol and imidazole.

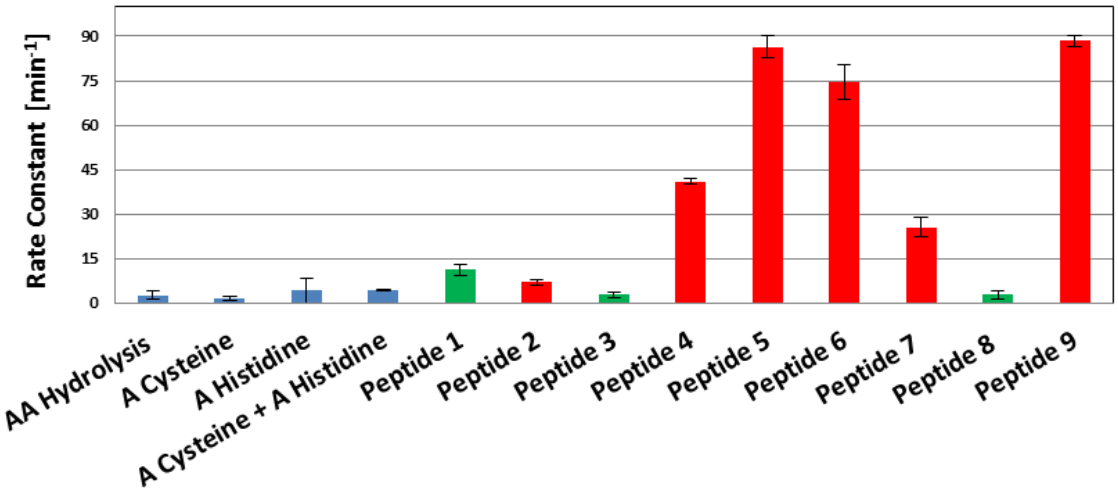

Figure 14: Deacylation rate constants of Peptide 1 through 9 and controls.

Figure 14 presents the first-order deacylation rate constants from the Ellman's reagent trapping study for Peptide 1 through Peptide 9 and its controls. The peptides that lacked histidine (green bars: Peptide 1, 3, 8) showed little increase in deacylation by Ellman's trapping over the controls. Peptide 2, which does have a histidine and cysteine with alanine spacing groups, showed only a small increase in deacylation. It seems that the spacing with alanine groups and other aspects of the structure do not allow close proximity of the thiol and imidazole groups. Peptides 4, 5, 6, 7, and 9 all showed higher deacylation rates, with Peptides 5, 6, and 9 possessing 20-30 times higher rates than the ACAH control. For Peptides 5 and 6, the improved deacylation rates are likely due to the

effect of the bulky phenylalanine groups improving proximity of the thiol and imidazole groups. The high rate for Peptide 9 may also be due to proximity, as well as the addition of two more histidine groups. Interestingly, Peptide 7 with the Phe-His-Phe-Cys-Ala-Gly-Asp in reverse order had a much lower rate. This reduction in deacylation may be due to the charge cancellation of the terminal Arg and Asp groups. Finally, considering that the deacylation rates were determined using very low concentrations of Ellman's reagent (400 μM) and peptide (100 μM), the actual acetyl group exchange rates in Peptides 5, 6 and 9 may be at least 100-fold higher than the observed deacylation rates.

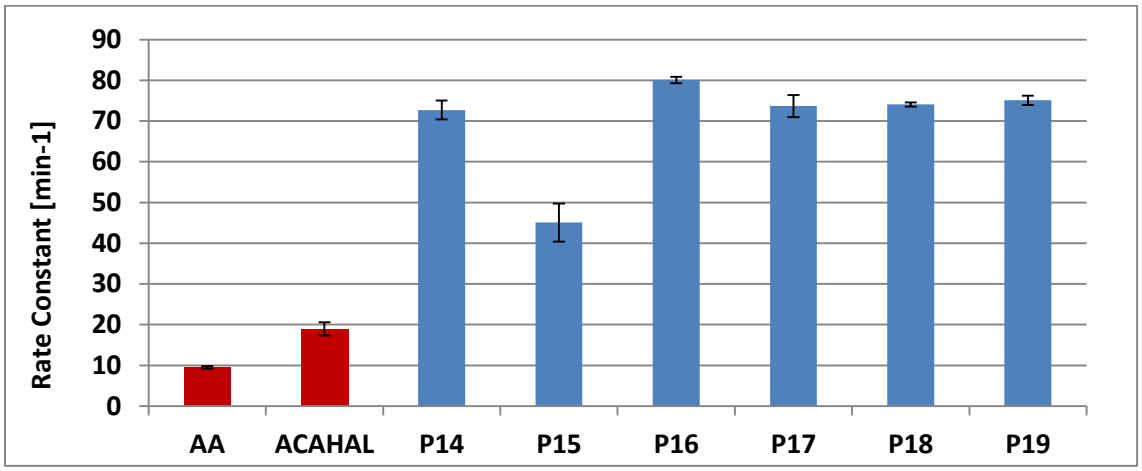

Figure 15: Deacylation rate constants of Peptide 14 through 19 and controls.

1.2.3 **NMR**

Figure 16 and Figure 17 show the direct results from NMR for acetyl-cysteine and acetyl-histidine respectively. Figure 18 shows the NMR half-height line widths corresponding to the protons on the β-carbon of cysteine and the ε-carbon of histidine residues at 2.82 ppm and 8.43 ppm, respectively. Overall, the half-height line widths of the peptide synzyme broadened for every peptide. However, broader line widths were

observed for Peptides 5 and 6, confirming that steric effects of bulky side groups bring the thiol and imidazole groups into closer proximity.

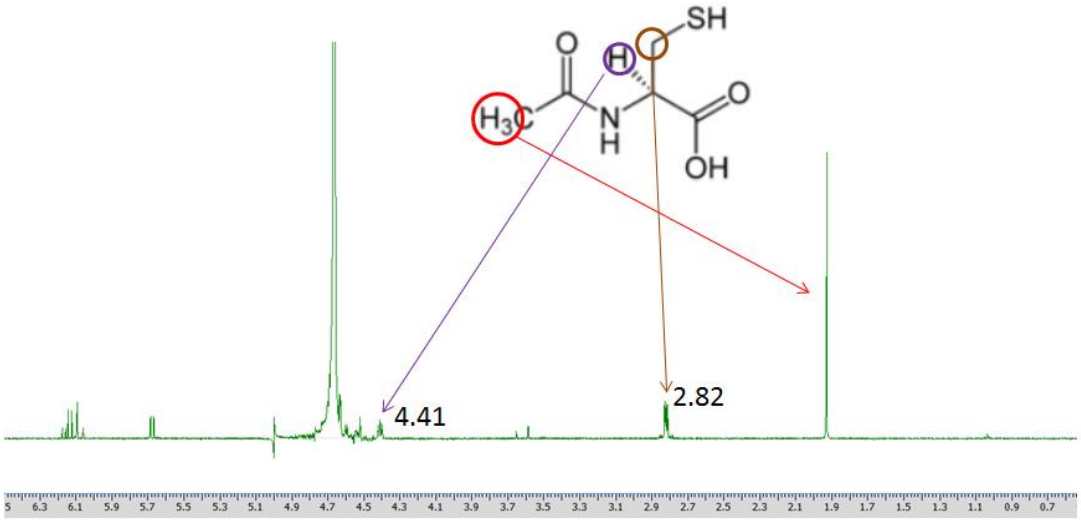

Figure 16: 1D proton NMR spectra of acetyl cysteine with labeled peak at 2.82 ppm corresponding to the β-carbon proton.

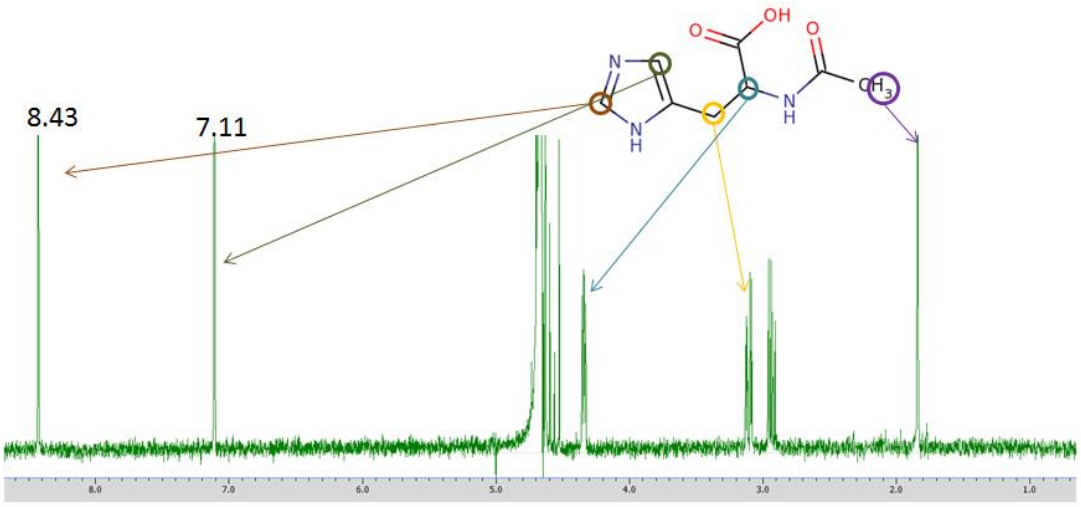

Figure 17: 1D proton NMR spectra of acetyl histidine with labeled peak at 8.43 ppm corresponding to the ε-carbon proton.

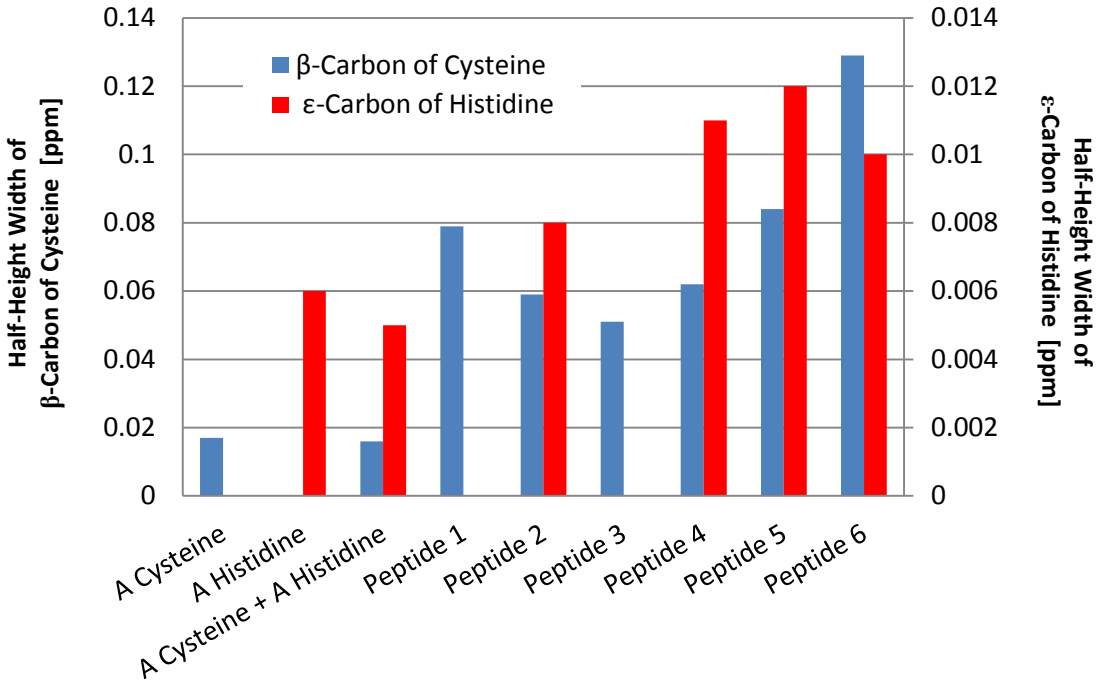

Figure 18: Half-height line width for proton on β-carbon of cysteine (blue) and on ε-carbon of histidine (red).

1.3 NAMD and VMD Modelling of the Peptide

1.3.1 System Setup

We used the CHARMM27 lipid parameter file (which pertains to the standard 20 amino acids) to quantify values used to calculate the force fields. Explicit solvent effects on the system are mimicked using the Generalized Born model, where the dielectric constants of the protein and solvent are 1 and 78.5, respectively. The ion concentration is set at 0.008 M along with a temperature of 293 K to reflect the 0.1x TB condition at room temperature. It should be noted that Peptide 9, which has three histidine residues instead of one, cannot be directly compared to the other peptides.

1.3.2 **Molecular Dynamics Simulation**

Five independent trajectories of 60 ns were performed for each peptide to analyze two distances: 1) the interresidue distances as the peptides experience conformational changes and 2) end-to-end distance to measure the overall peptide structure. The initial structures of all peptides were developed using Accelrys Discovery Studio 3.5. The time step size is 2 fs, dictated by the stretching frequencies of the peptide bonds (~10 fs). The system is minimized at 0 K for 100 steps of conjugate gradient. The target temperature of 293 K is controlled during 30,000,000 steps of equilibration using Langevin Dynamics with a damping coefficient of 1. To avoid instability at higher temperatures, the bonds connecting hydrogen to other atoms are constrained using the SHAKE algorithm. The cut-off and switch distances for nonbonding interactions are 14.0 Å and 13.0 Å, respectively. The conformations are saved every 250 steps or 5×10^{-4} ns while the energies are saved every 100 steps or 2×10^{-4} ns(38).

1.3.3 **NAMD & VMD Analysis**

Simulations were performed on the previously studied Peptides 2 through 9 as well as Peptides 14 through 19. Each simulation of 60 ns contains 120,000 distance values, taken between the lone nitrogen atom of histidine and the sulfur atom of cysteine for the Cys-His interresidue distances, and the carbon atom of the c-terminus and the nitrogen atom of the n-terminus for the end-to-end distances. The distance data were imported into Excel where they were plotted against time frames. Figure 6 shows Peptide 14 in VMD with the Cys-His bond length and end-to-end distances shown along with a plot of the Cys-His distance over 60 ns. Each simulation was run five times per peptide.

The two main differences between the model peptide and the actual experimental molecules are: 1) the missing acetyl-thiol or acetyl-imidazole group and 2) the acetyl terminated c-terminus. The simplified model may provide slightly unrealistic results since the interaction on which we are focusing occurs during the acetyl exchange. However, the general Cys-His measurement will give us insight as to how the neighboring residues affect the interresidue distance. The non-acetylated c-terminus may have a slight effect on the flexibility of the entire peptide, but we should see minimal difference for our end results.

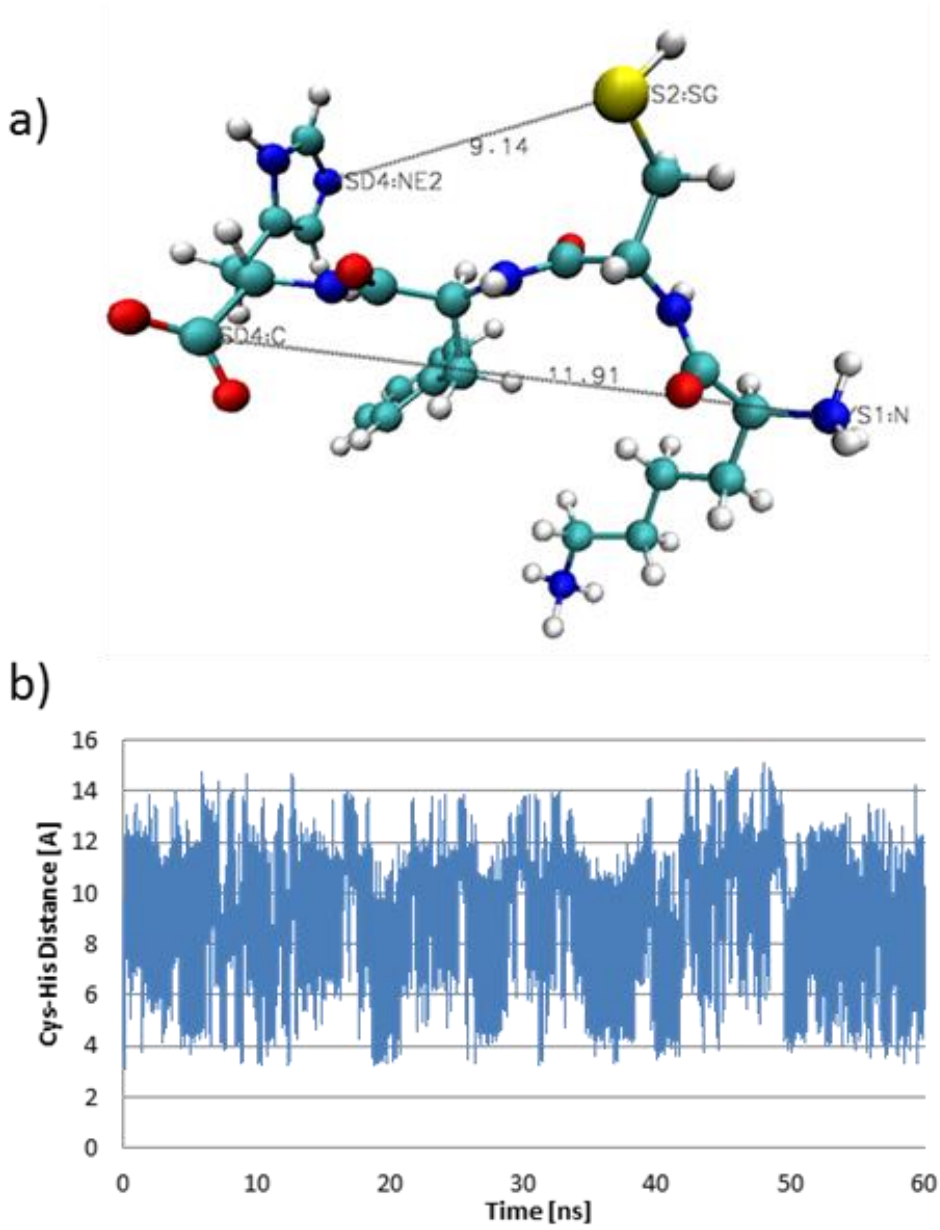

Figure 19: a) Peptide 14 shown in VMD with labelled Cys-His interresidue distance as 9.14 Å and end-to-end distance as 11.91 Å. b) Plot of 120,000 data points of Cys-His distance over 60 ns.

Upon obtaining the data, the Cys-His interresidue average distances were plotted for all peptides with the deacylation rate constants to check for correlation. We hypothesized that the smaller the interresidue distances of a peptide, the larger its corresponding deacylation constant due to the frequency of interaction between the

amino acids. However, the plot had a weak negative correlation with an R^2 value of 0.0025. Dividing the peptides between 2 through 9 and 14 through 19, the correlation was still weak at R^2 values of 0.20 and 0.21 respectively. The average distances for Peptides 14 through 19 increased from 9.24 Å to 9.88 Å with the exception of Peptide 15 with 9.14 Å.

Investigating further, we noticed a correlation between the Cys-His distance deviation, which shows the variability in the distances, and the deacylation rate constant. As plotted in Figure 20 , there is a strong correlation between the distance deviation and deacylation rate constants for Peptides 2, 4, 5, and 6. These peptides are very closely related in terms of peptide length, while the amino acid sequence only varies by the c-terminus amino acid (Gly, Arg, and Lys) and the amino acids surrounding the cysteine (Ala-Cys-Ala or Phe-Cys-Phe). Peptides 2 and 4 showed higher distance deviation than Peptides 5 and 6. This shows that the cysteine surrounded by alanine allows larger variability in intermolecular distances between the histidine and cysteine, which is unfavorable for the acetyl exchange. From this particular set of results, it may be concluded that smaller deviations in the Cys-His distance allow more interaction between the two residues due to the increased confinement in the structure.

From the same series of peptides, Peptide 9, which contains three extra residues and two more histidines, achieved a much lower Cys-His distance deviation at 1.20 Å, but only reached a deacylation rate slightly higher than Peptide 5. Also, Peptide 7, which has the reverse order of cysteine and histidine, and also a low distance deviation at 1.38 Å, had a poor correlation to its low deacylation rate compared to Peptides 2, 4, 5, and 6. This

shows that this method of correlation needs to be used with caution and may work best when peptides with very similar sequences are compared.

The Cys-His distance deviation and rate constants of Peptides 14 through 19 are plotted in Figure 8. The R^2 value for this correlation is 0.53, which shows mediocre correlation between the distance and the rates. However, it is notable that Peptide 15, which had the greatest distance deviation at 2.53 Å, achieved roughly half the deacylation rate constant as other peptides. This may indicate an existence of a threshold distance deviation that is necessary to achieve a certain rate constant. If the distance varies too much, this is an indication that there are fewer chances for the thiol anion to attack the acetyl-imidazole.

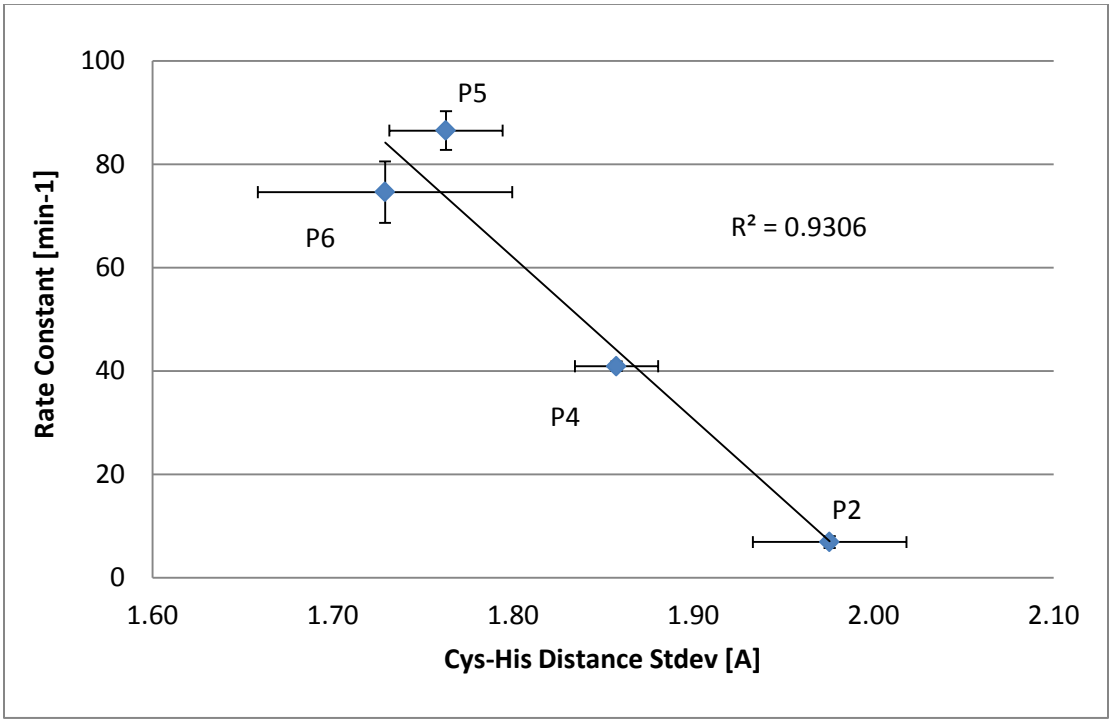

Figure 20: Cys-His distance deviation vs deacylation rate constant for Peptide 2, 4, 5, and 6.

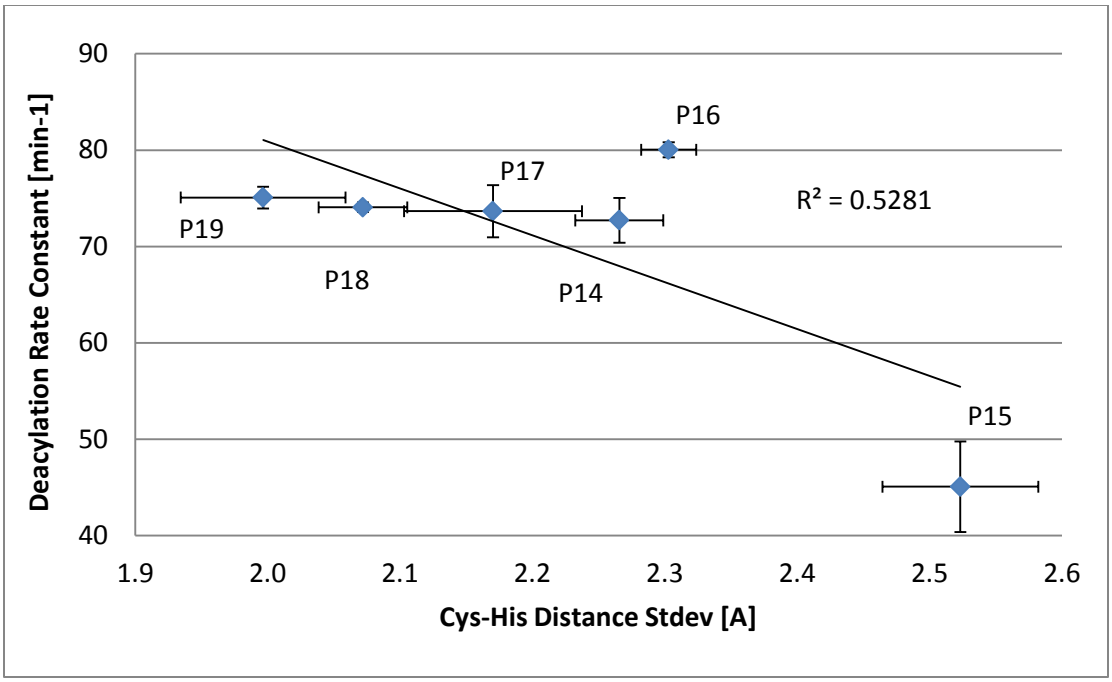

Figure 21: Cys-His distance deviation vs deacylation rate constant for Peptides 14 through 19.

Figure 9a shows the end-to-end distances of Peptides 14 through 19 in relation to the Cys-His distance deviation. It can be noted that longer peptides have a longer end-to-end distance, which contributes to a shorter Cys-His distance deviation. Longer molecules generally have less freedom to move due to their molecular strain30-33. A simple plot of number of amino acids vs the Cys-His distance deviation is shown in Figure 9b. This correlation achieved a high R^2 value of 0.74. Although it is possible to simply increase the length of the peptide, Peptide 9, which has three more residues than Peptide 5, only achieved a marginal rate increase. It is difficult to directly compare these two peptides since Peptide 9 also contains two extra histidine molecules that could react with the acetyl-thiol intermediate at any time. Further NAMD simulations with variations of peptide amino acid chain length and number of histidine molecules will be necessary to see the effect of the extra histidine molecules.

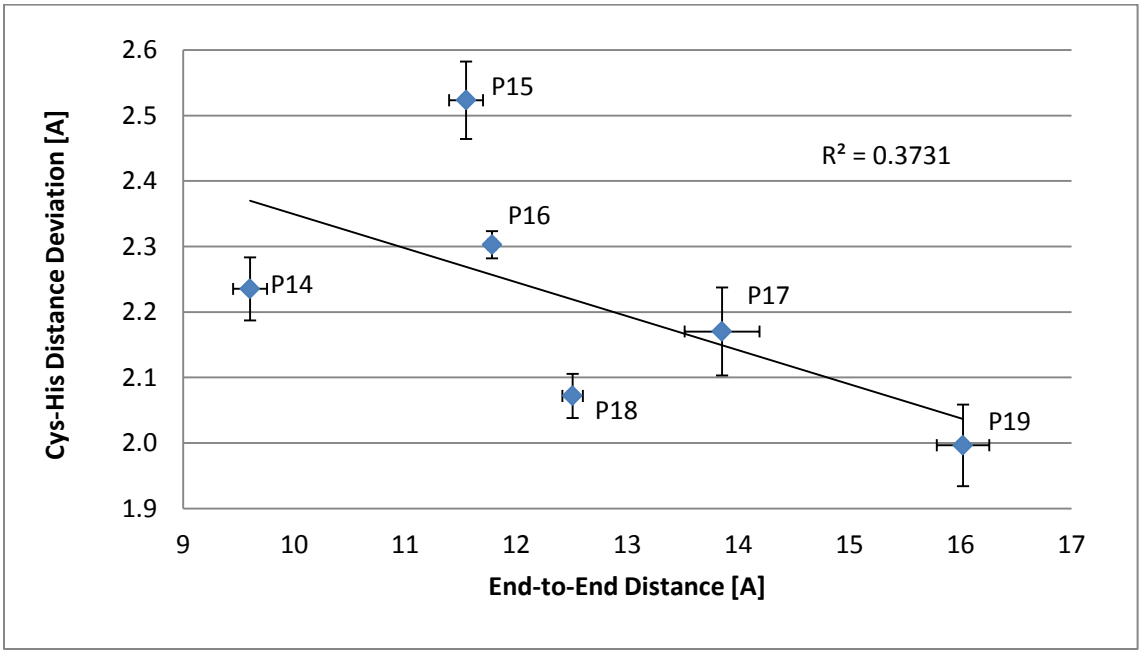

Figure 22: Peptides 14 through 19, end-to-end distance vs Cys-His distance deviation.

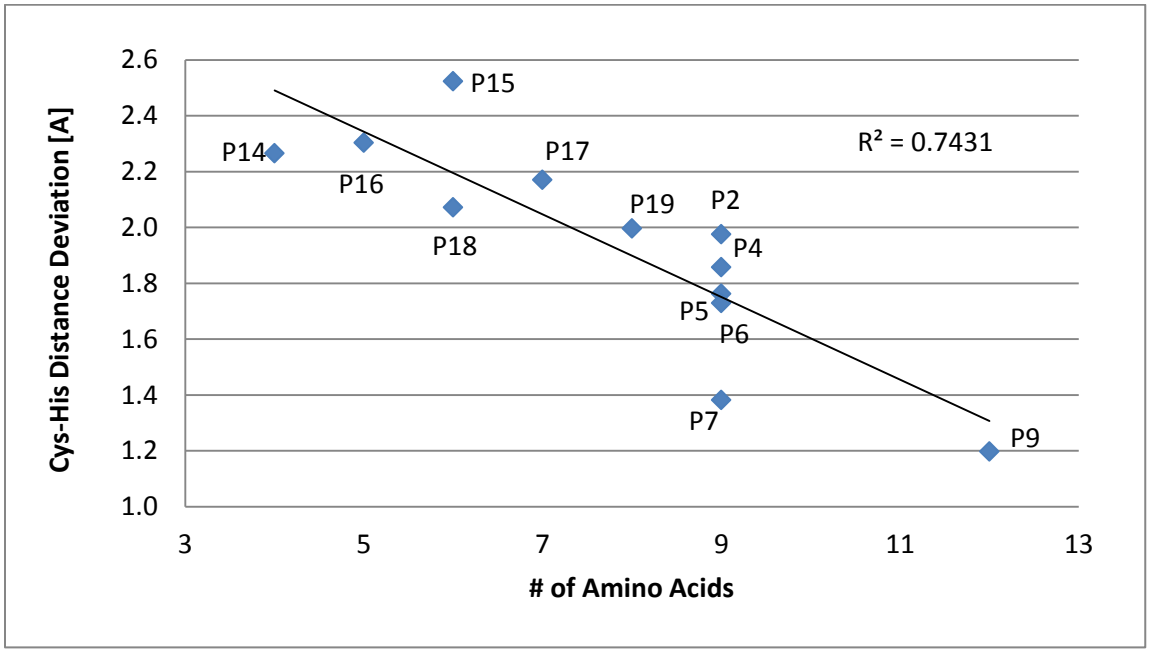

Figure 23: Number of amino acids vs Cys-His distance deviation for all peptides.

Table 2: Combined result showing peptide length, deacylation rate constant, Cys-His distance, and end-to-end distance.

			Cys-His Distance		End-to-End Distance	
Peptide Number	Amino Acid Length	Deacylation Rate Constant [min-1]	Average [A]	Deviation [A]	Average [A]	Deviation [A]
2	9	6.9	9.92	1.98	15.39	3.90
4	9	40.9	9.89	1.86	12.88	4.00
5	9	86.5	10.18	1.76	13.23	4.45
6	9	74.6	9.94	1.73	15.83	3.82
7	9	25.5	10.27	1.38	14.86	3.52
9	12	88.4	10.41	1.20	14.30	6.26
14	4	72.7	9.24	2.27	9.65	2.02
15	6	45.1	9.14	2.52	11.55	3.52
16	5	80.0	9.32	2.30	11.78	2.23
17	7	73.7	9.32	2.17	13.85	4.44
18	6	74.1	9.83	2.07	12.51	2.90
19	8	75.1	9.88	2.00	16.02	5.01

For a numerical point of view, Table 2 provides the compiled distance results and deacylation rate constants for each peptide.

1.4 Discussion

Fifteen peptides that contained various arrangements of cysteine, histidine, serine, and aspartate were studied: the key amino acids normally found at the active sites of proteases. The deacylation rates determined by Ellman's trapping reaction were highest for the cysteine, histidine, and aspartate containing peptides that had intervening phenylalanine groups. Peptide 6, 18, and 19 also had significant lowering of the cysteine thiol group pKa, indicating interaction between the thiol and imidazole groups. The broadening of the proton NMR line widths further supported a closer interaction of the cysteine and histidine groups in Peptides 5 and 6. The results demonstrate that the close proximity of a thiol and imidazole group produces a significant destabilization of the acyl-thiol intermediate, which is exhibited as a very rapid intramolecular acyl group exchange between the two groups. Nevertheless, the actual deacylation rate and turnover of the acyl-imidazole intermediate, without Ellman's trapping, is still very slow. This is

clearly due to the back-attack by the thiol nucleophile on the acetyl-imidazole intermediate. The role of the aspartate carboxyl group in this acyl exchange process is less clear. Overall, this study supports many of the key aspects of enzyme catalysis in proteases such as papain and chymotrypsin. It clearly emphasizes the importance of dynamic mechanisms in achieving the leaving group effect and producing turnover. It also suggests that the role of the histidine imidazole group as a nucleophile, rather than a general acid-base catalyst, should be reconsidered.

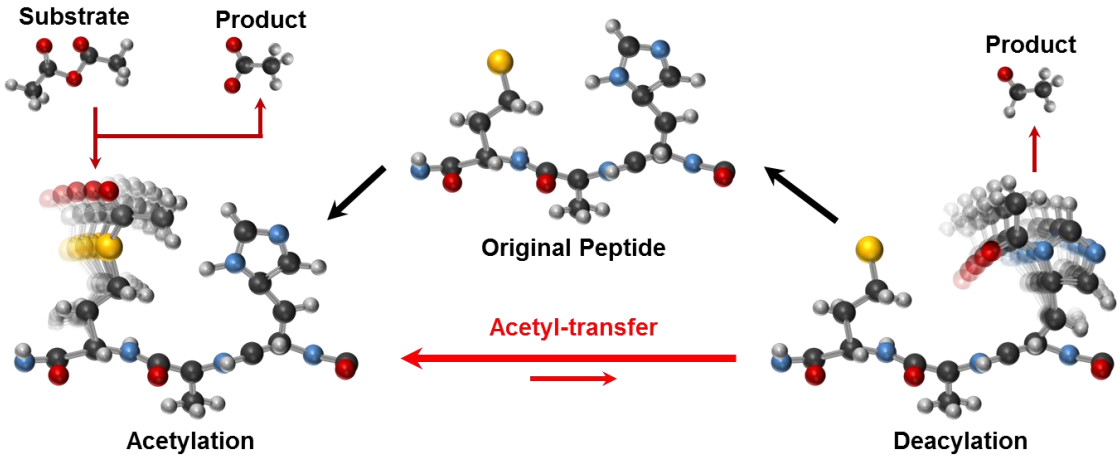

Figure 24: Scheme showing the movement necessary to overcome back-attack reaction of the cysteine thiol.

The Cys-His and end-to-end distance results from NAMD confirm that the acetyl transfer occurs at greater rates for peptides with a more confined geometry. There are several ways in which this can be achieved. The first is to apply a rigid structure intrinsically through the design process of these peptides. Like natural enzymes, a more precise interresidue location is necessary in order to let the acetyl transfer occur. Longer chains have proven that they can produce a more rigid Cys-His structure(39-41). Further incorporation of known structures such as protein folds and helixes may be helpful. Another method is to confine these peptides to objects with known boundaries and

configurations. This can be achieved by attaching one or both ends of the peptide to a structure such as a metallic surface or to nanoparticles. By anchoring the terminus of the peptide, the flexibility of the peptide will be greatly reduced, allowing a more controlled interaction between the amino acids. In addition to controlling one end of the peptide, attaching peptides on surfaces allows the application of other external forces (electric field, fluidic, or acoustic) that can be used to assist the mechanical activity of the peptides. Our present hypothesis is that the application of a directional oscillating or pulsing DC or AC electric field may ultimately provide the mechanism for preventing back attack and producing turnover. Chen et. al. has shown a sensor mechanism that measures for phosphorylated and non-phosphorylated peptides attached to a metallic surface by applying a DC voltage. The phosphorylated peptides collapse while the electric field is applied, but the non-phosphorylated peptides remain insensitive towards the field, allowing for kinase reactions to occur. Application of any form of external force adds a variety of parameters that can be adjusted. With the help of experimental and modelling data, these parameters can be tuned to control the peptide conformations and optimization becomes possible for many reactions. By further utilizing non-peptide based catalysts, such as metal ions, there are many possible forms of catalytic reactions possible.

Although we have been focusing on the rate at which the acetyl group transfers between the cysteine and histidine, our attention should also be on controlling the interresidue distance so that the deacylation process can occur from the acetyl-histidine as shown in Figure 4. To truly achieve this step, the interresidue distance must be increased to prevent the thiol back-attack from occurring. This is the opposite approach to our current studies, which focus on bringing the two residues closer to achieve higher

interaction. The level of control that is required to adjust these intermolecular distances at will is a challenging task and will require a smart design that allows peptide conformation to recognize and react to a certain binding pattern.

1.4.1 **Relation to IDP**

Although the crystal structures of proteins have been studied for decades, there has been an increased interest in proteins that contain disordered peptide chains during the binding process or the transition state of the reaction. These proteins are known as intrinsically disordered proteins (IDP) and are characterized by their lack of structure for some or all of their peptide chains, which assist reactions by creating different binding/inhibiting structures(42). While many focus on finding the crystal structure of the proteins, the known structures do not tell the full story of which protein produces its product. Specifically, there are proteins that start with an ordered state and transition through a molten globular state such as fd phage and histone octamer. There are also proteins that experience disorder to order transitions that allow for effective reactions, such as the transition of trypsinogen to fully active trypsin(43-45).

Our peptides are similar in concept with some of these IDPs; in order to achieve substrate binding and effective acetyl transfer, the peptides require low disorder. However, once the transition has taken place from acetyl-thiol to acetyl-imidazole, greater disorder is required to achieve deacylation. A possible solution for this process may be an additional charge-changing reaction that utilizes the rest of the inactive amino acids on the peptide chain, similar to the Asp-175 present in papain. Studies of these

proteins may help design a new set of proteins and enzymes that can produce catalysis through its controlled order/disorder.

1.4.2 **NAMD and VMD**

NAMD and VMD studies have been useful to view and calculate the movement of these peptides in a controlled environment. Although, these simulation results must be taken with caution because the parameters do not represent the experimental conditions perfectly, correlations can be made to a certain degree. The main difference between the modelling and the actual experimental condition is the acetylation of the thiol or the imidazole to represent the acetyl group transfer. For future studies, we plan to modify the thiol to an acetyl-thiol intermediate to see the change in distance that reflects a more accurate environment.

In papain, the Cys-His interresidue distance is roughly 6 Å when measured from the PDB crystal structure[27]. Although we could use this distance as a reference point to build our peptides, it should be keep in mind that the papain macromolecular structure produces precise movements during catalysis that we may not completely understand. From our results, it may be suggested that Asp-175 has little effect on the actual catalytic triad, which leads us to believe that the actual papain mechanism is dominated by the cysteine-thiol and histidine-imidazole interactions.

1.5 Conclusion

In conclusion, six new peptides were designed to test their reaction rates. The acetylation and deacylation rate constants showed consistency with previously studied peptides and confirmed the importance of steric hindrance created by the phenylalanine.

Furthermore, molecular dynamics simulations have shown signs of higher acetyl transfer rates related to the overall peptide length and the Cys-His interresidue distance deviation. Future peptides will be designed using modelling first to confirm a lower Cys-His distance deviation. Although our studies have focused on the acetyl transfer rate, it is important that future experimental designs be directed at achieving secondary conformational changes that lead to true catalytic turnover, i.e., deacylation without Ellman's Reagent trapping. Thus, future work will focus on both structural improvements and the application of external electric fields to produce desired nanomechanical properties for achieving turnover.

Chapter 2, in part, has been published in Catalysis Communications, "Quest for a turnover mechanism in peptide-based enzyme mimics," by T. Takahashi, M. Cheung, T. Butterweck, S. Schankweiler, and M. J. Heller (2015) **59**, 206-210, and has been submitted for publication in Biochemistry, "Molecular mechanical properties of short sequence peptide enzyme mimics" by T. Takahashi, B. C. Ngo, L. Xiao, G. Arya, and M. J. Heller (2015). The dissertation author is the primary investigator in these publications.

3

Heterogeneous Peptide Catalysis

Studies on catalysis with in which the peptides are attached to surfaces or included in structures to create a more controlled environment are shown in this chapter. These structures include micelle, nanoparticles, and flat surfaces. In addition to the structural control of the peptides, we studied the effect of induced electric field in order to take advantage of the charged molecules of specific amino acids to precisely align the peptides.

1.6 Electric Field Introduction

1.6.1 Previous Studies

The use of electric field to control molecules in various environments has been studied for decades. In relation to biological molecules, electric field has been used to flow charged molecules through mediums, control conformational changes, or collect and separate molecules with varying dielectric properties. Interests to study the effect of electric field on cells, DNA, RNA, peptides and proteins have increased due to its ability

to control the structures of molecules permanently or intermittently with great control. In 1972, Neumann showed that pulsed electric field (PEF) of 20 kV/cm is capable of producing long-lived changes in ribosomal RNA by creating dipole moments by shifting the ionic atmosphere of multi-stranded polynucleotide helices which causes unwinding(46). Recently, electric field has been used to inactivate enzymes through change in protein charge configuration. This has been useful in the preservation of certain food products such as milk which contains lipase and alkaline phosphatase. Others have found enzymes that can be deactivated by electric field within horseradish, wine, and sugar beet pulp, and various food groups. There are varying theory as to how the electric field pulsing inhibits reactions. For example, acetic acid esterification is possible by increasing the energy of and adding vibration of hydrogen bonds that keeps the ethanol and acetic acid together. This vibration frequency produces the resonance phenomenon resulting in the breakage of the hydrogen bond, freeing the two molecules. Although the mechanism for the PEF inactivation of many enzymes and food products is not fully known, many studies suggest conformational changes and denatured state of the protein. Several studies have shown that electric field strength, pulse duration, number of pulses, and pulse shapes are the main variable that affects the protein conformation. In 2012, Chen et. al. found that they can coil and stretch phosphorylated peptides attached to gold surfaces by applying positive and negative DC voltage(47). This allowed the detection of charge-related biomolecule conformations of various peptides(48-61).

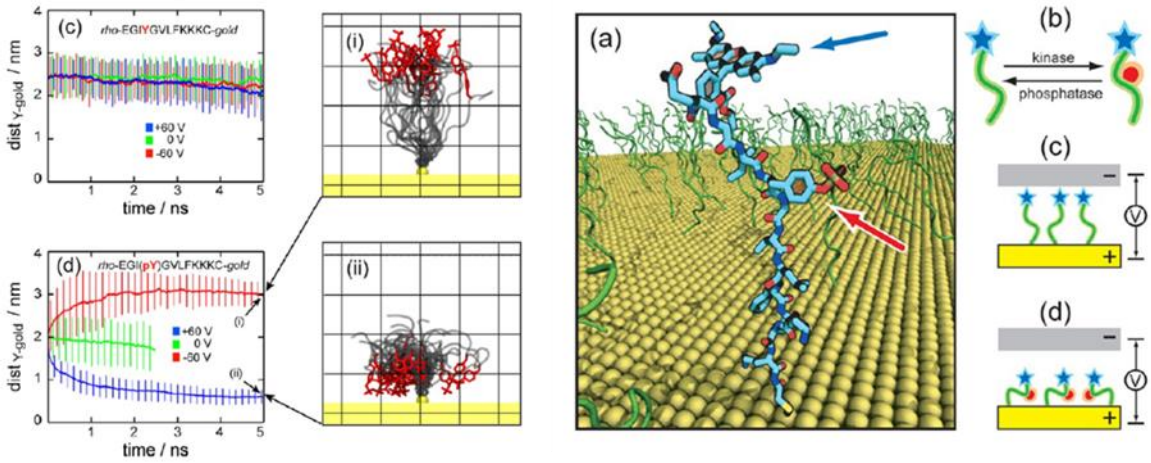

Figure 25: Example of electric field perturbation by Chen et. al.

1.6.2 Electric field application on cysteine protease mimics

Although these are examples in which electric field is applied on enzymes, they have the function of inactivation rather than activation or increasing the rate at which these enzymes function. The former is a much simpler process since it only requires the reduction of the structural integrity of the original protein. In order to achieve higher turnover rate, the applied electric field must cause molecules to align in a more precise conformation. This requires specifically knowing the target charge, charge orientation, charge distribution, and the timing at this charge exists within the molecule. These information are not easy to find, but based on our previous experiments, we have developed a method in which we can apply an electric field at the right moment on our cysteine protease mimics to achieve a higher turnover rate by overcoming the back-attack problem.

Figure 26 shows the schematic of how electric field can be applied to control the conformation of the cysteine and the histidine on a single peptide. In each step, a peptide

is shown with the one end of the peptide backbone attached to a support layer and cysteine and histidine shown individually. Step 1 through 3 shows the general nucleophilic attack from the thiol (S-) onto the substrate and the acetyl transfer that takes place from acetyl-thiol to acetyl-histidine. We have noticed that there is a positive charge difference created at the center of the imidazole when the acetyl group is attached and the addition, the free thiol contains a negative charge, which in the case of a back-attack, reacts with the acetyl group once again. However, if there is an electric field applied on the acetyl-histidine, the different charge on the imidazole and the thiol can be used to pull the peptides away from each other. This will result in a distance between the Cys-His which is too large for the cysteine to attack the acetyl-imidazole, allowing the acetyl group to deacylate. Upon deacylation, the peptide will return to its original state and continue to react with a new substrate molecule as shown in step 6.

The critical part of this separation of charge with applied electric field is the timing at which this field is turned on. Currently, we do not know the rate at which this transfer rate occurs since the Ellman's reagent deacylation rate experiments are not absolutely representative of the rate at which an acetyl-histidine group exists. Meaning, during the previous deacylation experiments, Ellman's reagent will only capture the free thiol only when the molecules are close enough to react. This leaves many chances of acetyl group exchange to occur before there is a free thiol that the Ellman's reagent can react. We have assumed that in order to capture every moment at which an acetyl group stays with the histidine, a nanosecond electric field pulses are necessary. Although we have the capability to produce these electric field pulses, it becomes difficult and expensive to apply these electric fields. Also, since there is never an instant when the

numerous peptides attached to surface are at the same step of the reaction, it is inefficient to target one instance of the reaction. Our experiments were performed on function generators which have the capability of applying up to 10MHz in frequency.

The significance of this approach is that unlike any other electric field application, it allows control of charges at the molecular level in order to enhance the target reaction rate. The idea that electric field can move charged molecules has been exploited for centuries; however, there has never been an instance in which it was used to ameliorate chemistry in a mechanical manner in order to overcome an uphill reaction. This method is the first application of electric field in order to produce minute conformation changes, similar to existing enzymes, in order to produce turnover. In addition to the application of mimicking cysteine proteases, electric field can be applied to any reaction that known charge differences exist within a molecule. More sophisticated forms of electric field application are listed in the Chapter 5.

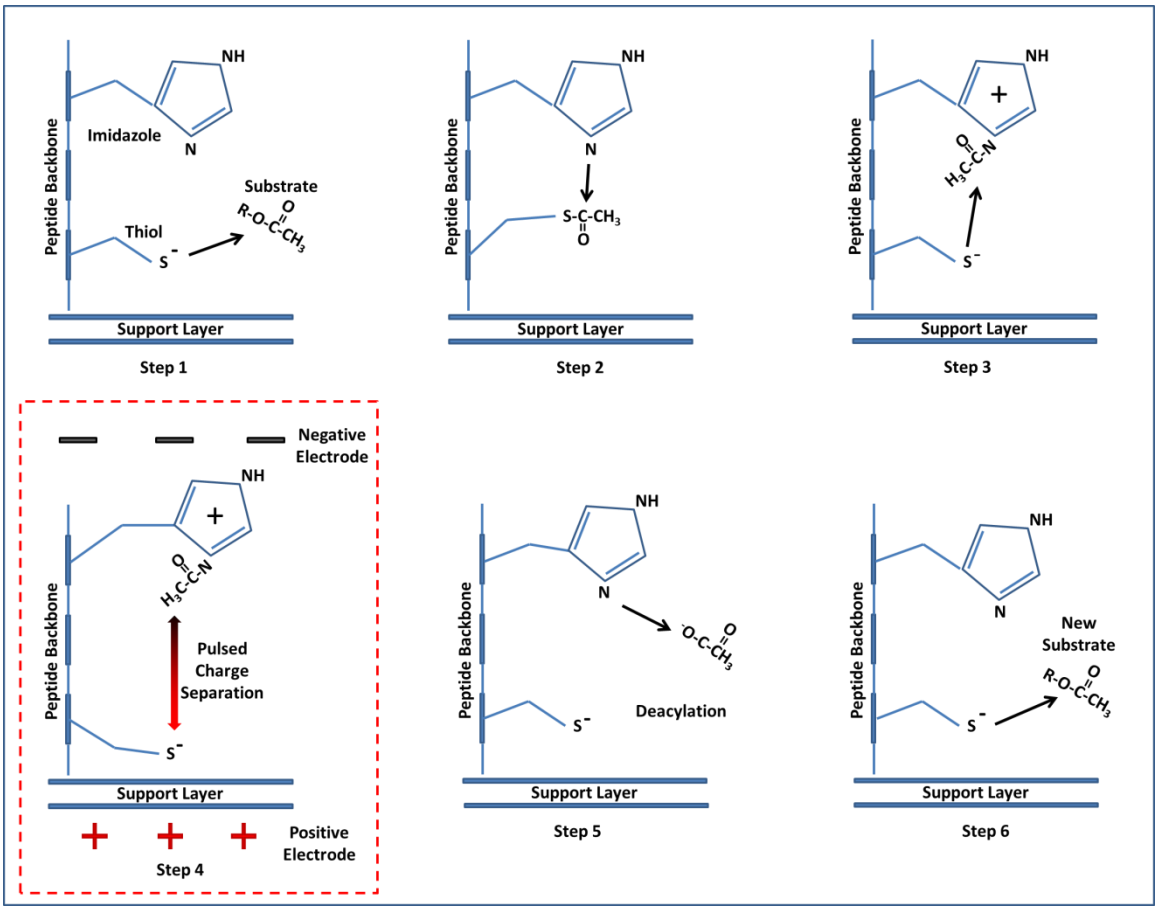

Figure 26: Scheme of electric fielding pulse controlled deacylation of cysteine-histidine peptide.

We would like to once again reiterate the difference in homogeneous and heterogeneous catalysis while explaining the advantages and disadvantages of applying electric field. In homogeneous catalysis, there are large number of interactions taking place between the peptide and substrate which allows simple measurements of the reaction rate in any number of volumes. However, the peptides are too flexible for electric field to be applied properly in a controlled manner and the high precision of charge-electric field interaction will not be achieved. In contrast, heterogeneous reaction which utilizes peptides attached to the surface can maintain a much more rigid conformation of the peptide. This allows precise orientations of the charges and reaction

sites. This precision comes with the shortcomings of having fewer interactions between the peptide and the substrates since bulk of the substrates will stay in solution far away from the surface of the peptides. In the later sections of the chapter, we will explain our attempt to combine homogeneous and heterogeneous interactions by using micelle structures and gold/polystyrene nanoparticles.

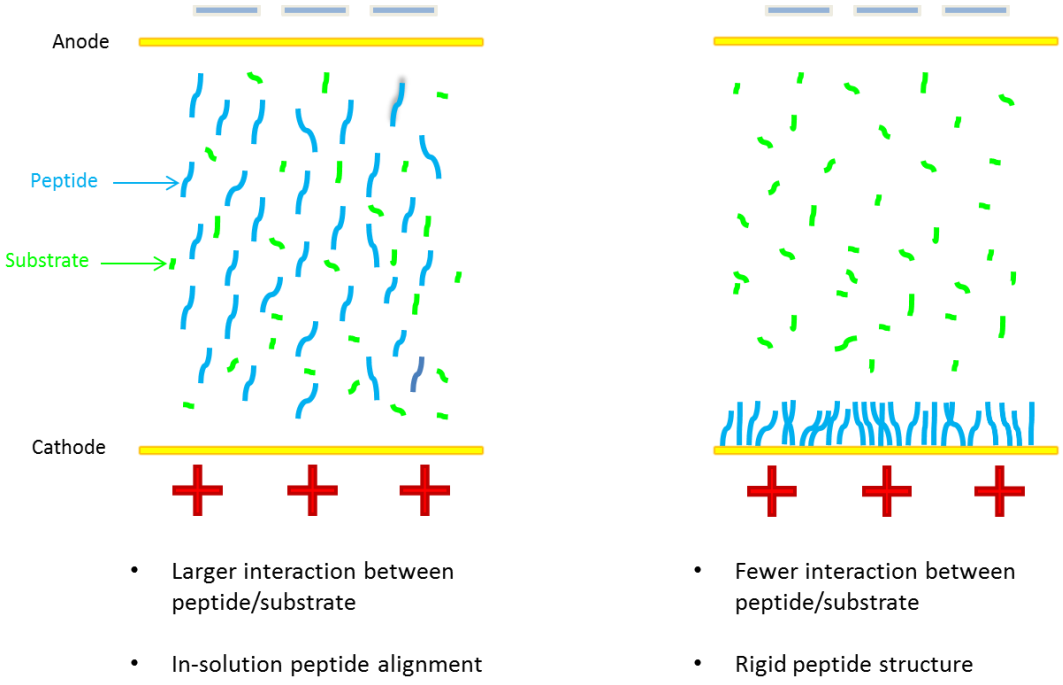

Figure 27: (left) Homogeneous and (right) heterogeneous catalysis with electric field.

1.6.3 **Homogeneous Electric Field Catalysis**

Knowing these facts, our original plan was to attempt to apply electric field on the previously studied peptide, Peptide 1 through 9, in order to create perturbation on the entire peptide backbone. These peptides were designed with specific charges placed at the ends of the peptide. For example, Peptide 6 contains a lysine which is a positively charged amino acid at its c-terminus and an aspartic acid at its n-terminus. The goal of

these peptides, in addition to studying the effect of phenylalanine steric hindrance was to align the peptides by applying an electric field to pull these charges apart and pulling the peptide backbone. The list of Peptide 1 through 9 is shown in Table 3 with positive (red) and negative (green) charges labelled for each.

Table 3: List of Peptide 1 through 9 with labeled positive (red) and negative (green) charged amino acids.

Number	Sequence
Peptide 1	Gly-Gly-Ala-Ala-Cys-Ala-Ser-Ala-Asp
Peptide 2	Gly-Gly-Ala-Ala-Cys-Ala-His-Ala-Asp
Peptide 3	Arg-Gly-Ala-Ala-Cys-Ala-Ser-Ala-Asp
Peptide 4	Arg-Gly-Ala-Ala-Cys-Ala-His-Ala-Asp
Peptide 5	Arg-Gly-Ala-Phe-Cys-Phe-His-Ala-Asp
Peptide 6	Lys-Gly-Ala-Phe-Cys-Phe-His-Ala-Asp
Peptide 7	Arg-Asp-Phe-His-Phe-Cys-Ala-Gly-Asp
Peptide 8	Arg-Asp-Phe-Asn-Phe-Cys-Ala-Gly-Asp
Peptide 9	Arg-Gly-Gly-His-Phe-Cys-Gly-Pro-Gly-His-Gly-His-Gly-Asp

The first attempt towards electric field enhanced catalysis was performed in a homogeneous setting directly inside a 1 cm by 1 cm standard quartz cuvette for UV-Vis spectrophotometer as shown in Figure 28. Two capillary tubes of different length which contained an agarose gel plug and 1x PBS buffer above were inserted in the cuvette. Once the platinum electrodes were inserted, a potential difference was applied, creating an electric field from one end of the capillary tube to the other. Figure 29 shows the 3-dimensional electric field concept using the same UV-Vis cuvette. It is beneficial to use the UV-Vis cuvettes since they come in standard sizes and allows for real time measurement of the reaction.

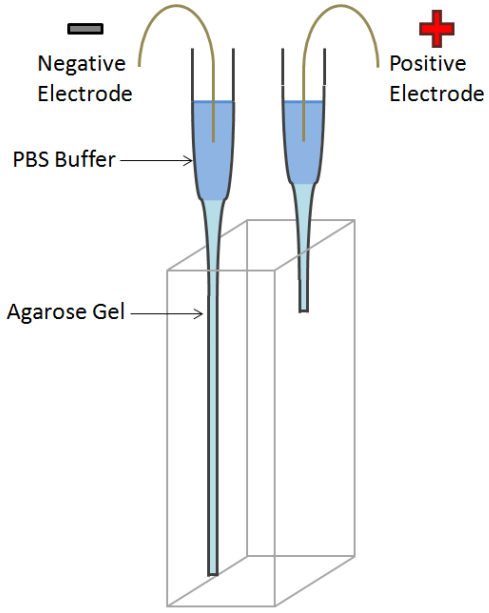

Figure 28: Initial electric field setup directly in the UV-Vis cuvette. Two glass capillary tubes filled with agarose gel and PBS buffer were inserted in the cuvette.

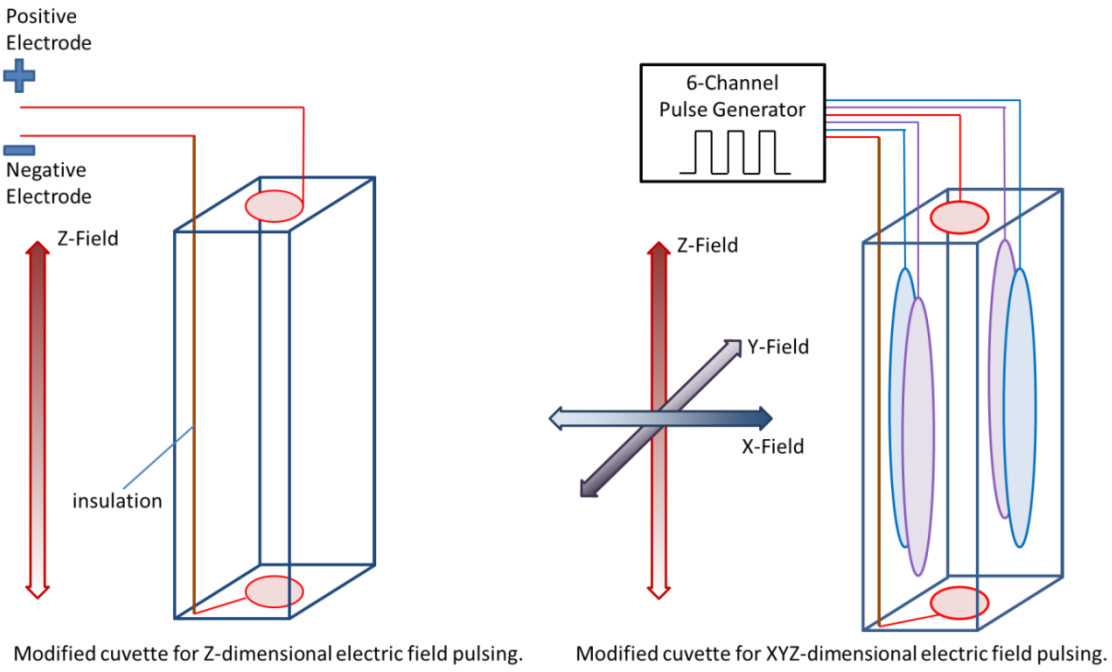

Figure 29: Electric Field induced within a UV-Vis cuvette in z-dimension (left) and xyz-dimension (right).

We managed to use this configuration to perform tests with electric potential up to 200 V. Below are the results for Peptide 2 pulsed at 100 Hz at varying voltage (Figure 30) and Peptide 6 and 7. The acetylation experiments were carried out similarly to the procedures listed in section 1.1.2 with the same concentration of the substrates and enzymes. For Peptide 2, the electric potential was raised to 400 V; however, the results were unattained due to the melted gel releasing the PBS buffer above. At higher voltages, noticeable heating had occurred and weakened the gel. At 200 V, the acetylation rates are noticeably higher, mainly due to heating of the substrate which causes the hydrolysis rate to increase and highly unlikely that enzymes were functioning under electric field as we hoped initially. In order to avoid the joule heating of the solution, we maintained our voltage under 10 V. For Peptide 6 and 7, we compared the measurements with ACAH rate under the same condition and adjusted the frequency at which the PEF was applied. Peptide 6

had a maximum absorption increase rate at 100 kHz while Peptide 7 had a maximum at 1 kHz. Although there were slight changes, these results were not statistically significant. We also realized the inaccuracy of the experimental setup using the capillary tubes and the electrodes since the distance between the platinum electrodes were never consistent. In order to simplify the experimental setup and achieve a more controlled environment for the peptide conformation, we moved on to different forms of fluid chambers and structures used for the peptides.

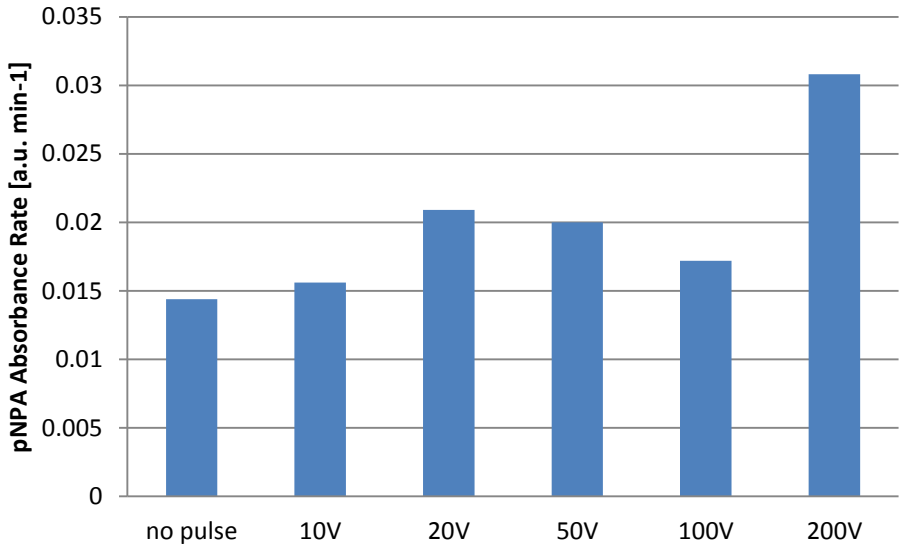

Figure 30: Peptide 2 acetylation rate with varying voltage at 10 kHz.

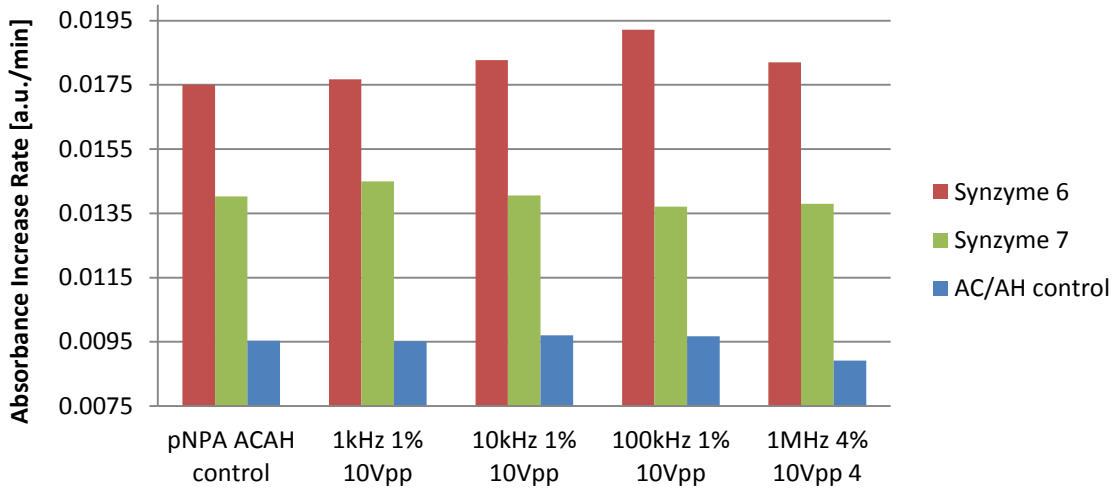

Figure 31: Peptide 6, 7, and ACAH control reacted with pNPA with various frequency pulsed electric field.

1.7 Micelles

Micelles are ubiquitous in biochemical reactions as small amphiphilic molecules can produce structures as large as lipids that are organized in a concentrated manner. Micelles maintain its structure by having an amphiphilic tail-head structure and depending on the hydrophobicity/hydrophilicity of those ends micelles will form above a certain critical micelle concentration. Micellular catalysis is a known phenomenon in which the addition of micelle structures affects the reaction rate and rate constants of organic reactions by utilizing its physicochemical properties and intermolecular interactions. Although not perfectly heterogeneous (no permanent structures or bonds), micelles form spherical structures that has the ability enhance the stability of the peptides.

The incorporation of the peptides into micelles may enhance reaction rates by providing a local hydrophobic environment within a surrounding aqueous phase. Many substrates of commercial or scientific interest, such as triacylglycerols, are at least somewhat hydrophobic and may partition into a micelle, thus concentrating near the

peptides contained in the micelle. The greater local concentration of the substrate would enhance the rate of catalysis based on the law of mass action(62-67).

1.7.1 **Experimental Methods**

There are two possible ways to create micelles that contain short-sequence peptides. One is to use existing micelle structures with known critical micelle concentrations and adding the peptide molecules in the micelle structure. In our experiments, several known surfactants were used in our experiments, including: Triton X-100, Tween 20, and Tween 80. Another method is to create amphiphilic molecules that include hydrophilic ends that contain the peptides with catalytic sites. For our experiment, we designed peptides with Palmitoyl group at the n-terminus which allows the peptides themselves to form micelles within the solution.

Table 4shows the list of substrate, controls, and sequences of Peptides 20 through 25 used for this experiment. Peptides 20 and 21 are intended to be used together to allow interaction between the two different peptide strands. Peptides 22 through 25 contain both cysteine and histidine groups to allow intra-peptide reaction as presented in the previous chapter. Peptides 22 and 23 differ in the order of the cysteine and histidine residues and Peptides 24 and 25 include an amine terminated c-terminal. We are expecting a difference in the critical micelle concentrations for these peptides with these variations in the c-terminal. Palmatic acid was chosen as the control that represents the peptides without its catalytic groups in addition to n-acetyl l-cysteine and n-acetyl l-histidine. Fluorescein diacetate (FDA) was chosen as the substrate since it is a harder substrate to hydrolyze and provides sufficiently distinct emission peaks(68-70). 0.01 mM

FDA was used while varying concentrations of the controls, peptides, and surfactants were used. Each reaction took place in 600 uL of total solution. 0.1x TB at pH 8.5 was used as the buffer. Each control was initially prepared by the addition into the buffer. 30 seconds after the addition of 0.01 mM FDA, the first time point was taken with Perkin Elmer LS 50 Fluorometer at 380 nm/515 nm excitation and emission.

Table 4: List of chemicals for the micelle experiment.

	Compound/Sequence
Substrate	Fluorescein Diacetate (FDA)
PA	Palmatic Acid (PA)
ACAH	Acetyl Cysteine + Acetyl Histidine (ACAH)
Buffer	Tris-Borate (TB)
Peptide 20	Palmitoyl-His-COO-
Peptide 21	Palmitoyl-Cys-COO-
Peptide 22	Palmitoyl-Cys-Phe-His-COO-
Peptide 23	Palmitoyl-His-Phe-Cys-COO-
Peptide 24	Palmitoyl-Cys-Phe-His-CO-NH2
Peptide 25	Palmitoyl-His-Phe-Cys-CO-NH2

Figure 32 shows the scheme of Triton X-100 and Peptide 22 interacting with a triacylglycerol molecule. The goal is to use the Triton X-100 as the base micelle structure and to imbed the peptides and the triacylglycerol alkane chain within the micelle structure. Figure 33 shows further example of the triacylglycerol molecule getting imbedded into the Triton X-100/Peptide 22 micelle structure. In addition, the active site of the synzyme, which is the relatively hydrophilic peptide portion, is concentrated at the outer edge of the micelle as is the relatively hydrophilic part of the substrate, which contains the ester linkages. The positioning of the labile ester linkage near the active site of the synzyme also serves to enhance the reaction rate. Once the lipase reaction occurs cleaves the glycerol bonds, individual strands of stearic c-18 fatty acids will be available

for further downstream reactions. In this example, the final reaction is to produce unsaturated fatty acids products such as omega-3 fatty acids. Other possibilities of future application include linolenic acid, eicosapentaenoic acid (EPA) and docosahexaenoic acid (DHA).

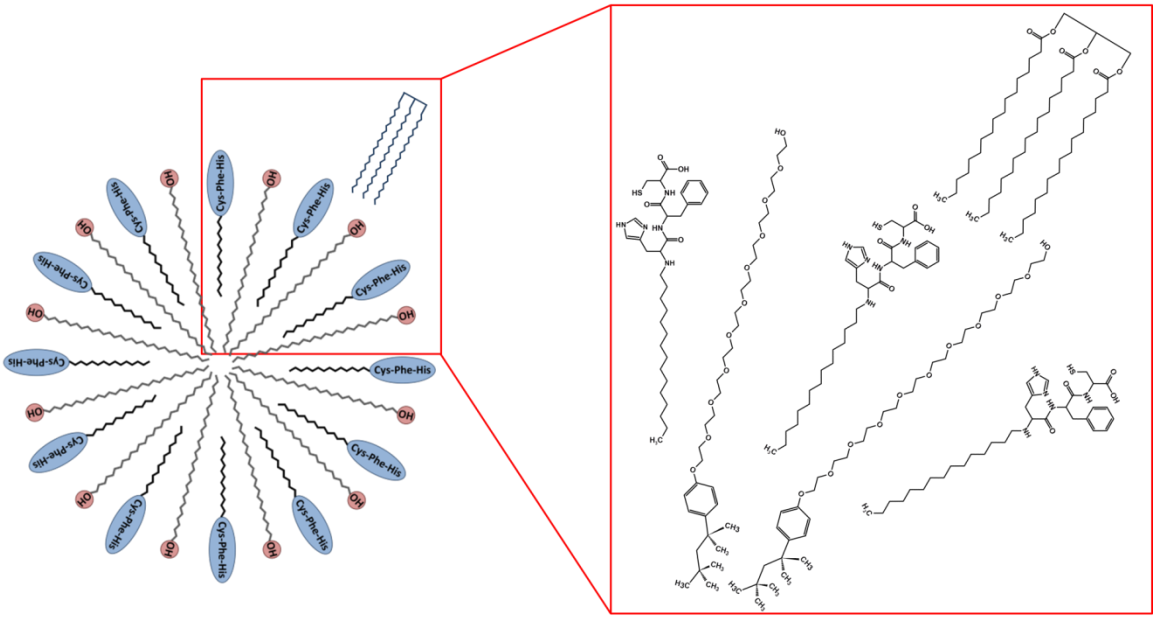

Figure 32: Scheme of micellular peptides interacting with alkane chains of triacylglycerol.

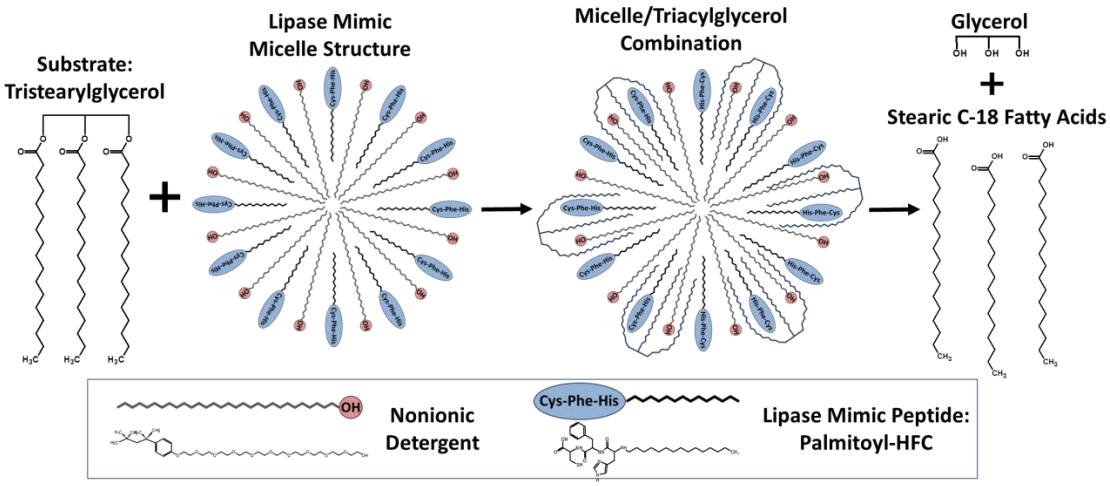

Figure 33: Peptide mimic of a lipase contained in a micelle.

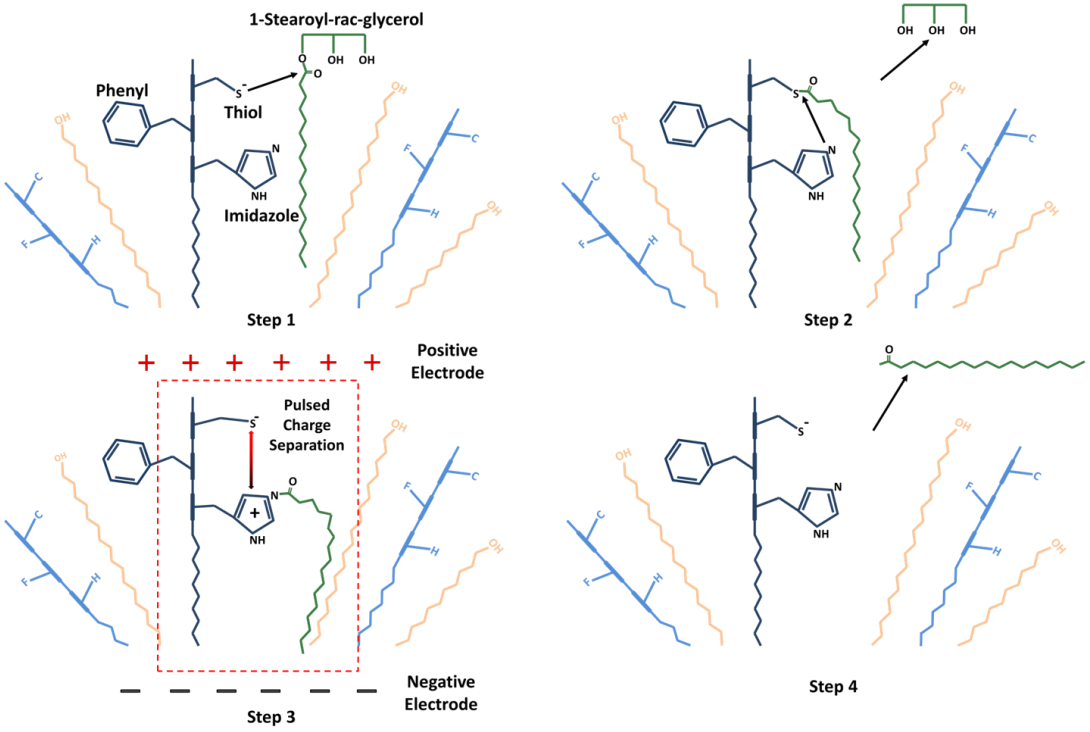

Figure 34: Electric field induced deacylation in peptide micelle.

Peptides embedded in micelles can also be combined with the use of an alternating electric field to achieve further rate enhancement. In Figure 34 step 1, the acyl-glycerol substrate is added while the electric field is not applied. The sulfur anion is

able to react with the ester bond and acquires the fatty acid as an acyl group. In step 2, the acyl group is transferred to the imidazole group. In step 3, the electric field is activated to pull the negative charge on the sulfur away from the positively charged acyl-imidazole, thereby preventing back-transfer of the acyl group to the sulfur. In step 4, the fatty acid is released from the imidazole into the surrounding medium. This scheme is similar to Figure 26 which has the peptide backbone attached to a rigid surface. Due to the inherent flexibility of the micelle structure, the Cys-His interacts not only within each strand, but with other strands as well. Micelle structures have molecules moving in and out of the micelle at any time. This flexibility is a key point when focusing on the deacylation aspect which requires the acetyl-imidazole group to move away from the cysteine to avoid back-attack.

1.7.2 **Results**

Figure 35 shows the rate of fluorescence increase through the acetylation from 0.1 mM FDA reacted with controls and peptides at 1.7 mM. Each condition was tested with and without the addition of 5 mM Triton X-100. Looking at the controls, there is a definite increase in the reaction rate once ACAH is introduced in the solution. This small increase in rate is due to the negative thiol anion (S-) producing a nucleophilic attack on the acetate molecule. As expected, the addition of the palmatic acid has no effect in creating a micelle on its own and has no effect on the overall FDA hydrolysis rate. Upon adding 5 mM Triton X-100, the rate remains the same for the controls. Palmatic acid still has no improvement on the rate, but rather slows the reaction down further even with the addition of Triton X-100.

From Peptides 20 through 25, various observations can be made. First, Peptides 20 through 23 show no increase when directly added with FDA. Once the Triton X-100 is added, Peptides 20 and 22 show an increase with Peptide 20 reacting three times faster than Peptide 22. Similar pattern can be seen with the combination of Peptide 20 and 21. In contrast, Peptides 24 and 25 show high reaction rates even without the addition of Triton X-100 and once it is added, a slight decrease in rate occurs.

Figure 36 shows the FDA acetylation rate with 0.01 mM FDA and 0.002 mM controls and peptides, with 5 mM Triton X-100. The ratio between substrate:enzyme:surfactant is 5:1:2500. In this case, the results look dramatically different with the peptides not showing great enhancement in acetylation rate. Although dramatic increases are not seen, Peptides 20, 21, and 22 with Triton X-100 show statistically significant increases compared to the controls.

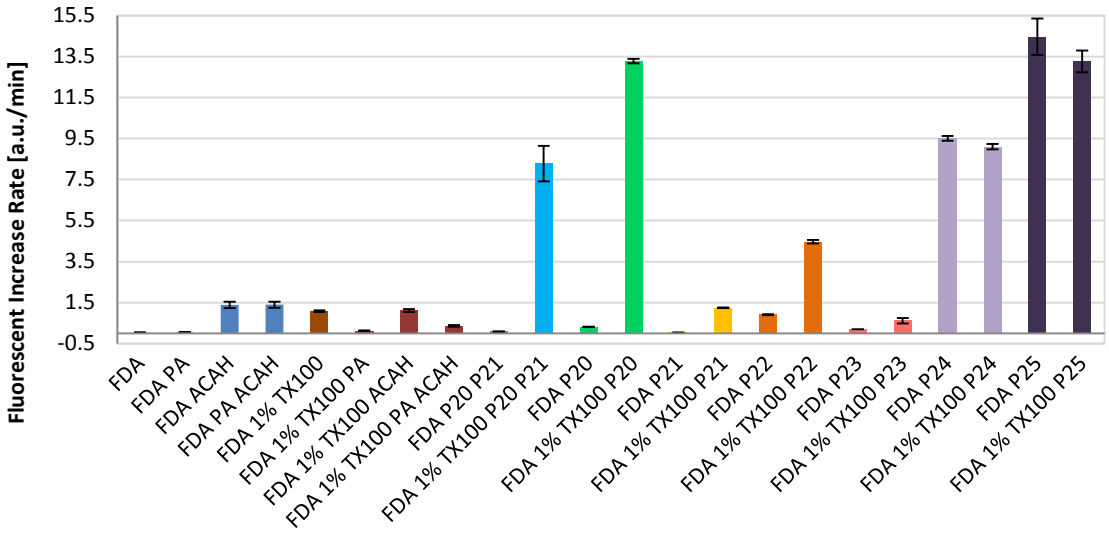

Figure 35: 0.1mM FDA acetylation rate with 1.7mM of controls (ACAH/PA/5mM Triton X-100) and Peptide 20 through 25.

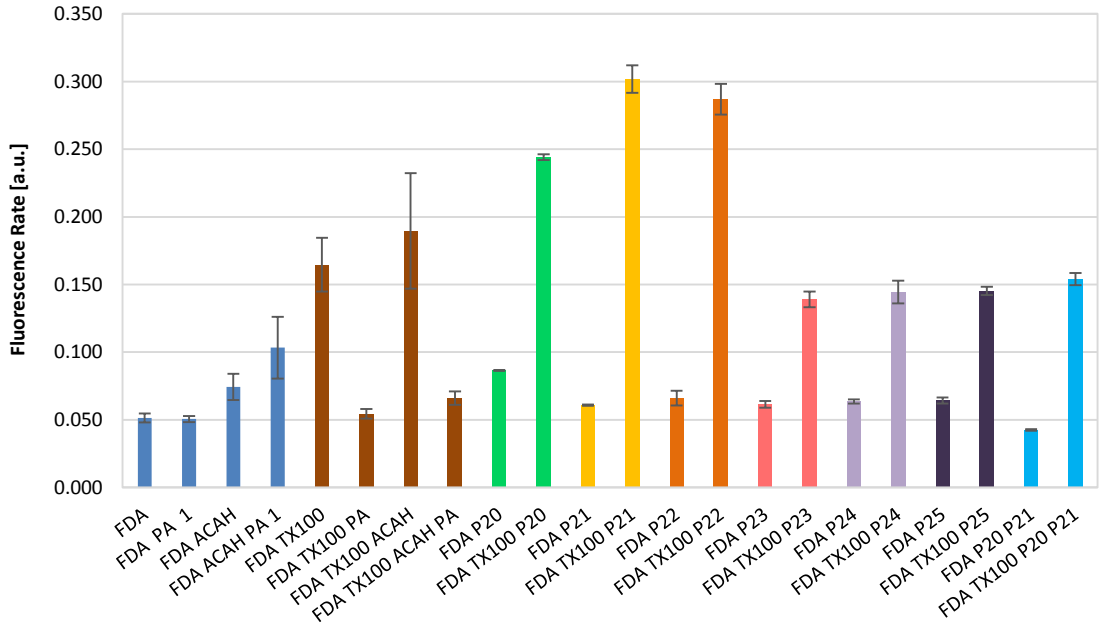

Figure 36: 0.01 mM FDA acetylation rate with 0.002 mM of controls (ACAH/PA/5 mM Triton X-100) and Peptide 20 through 25.

1.7.3 **Discussion**

The results from Figure 35 show that with a sufficiently high concentration of peptides, they can be incorporated into micelles with Triton X-100. Although Triton X-100 shows slight increase in acetylation rate, there is a significant effect seen from certain peptides being added. The most notable peptide is Peptide 20, which only contains a histidine residue and was originally planned to be used in conjunction with Peptide 21. However, the results showed that Peptide 20 worked better without Peptide 21, which contains the cysteine molecule that assists the reaction with its nucleophilic attack. This may be explained by several ways. First, the Triton X-100 molecules are controlling the peptides efficiently by allowing the palmitoyl ends to be inserted within the micelle structures while exposing the amino acid ends. Peptide 20 contains a histidine molecule which inherently can assist in catalysis. This has been noticed in many previous cases

that histidine molecules have been used to catalyze certain reactions. It is possible that the organization of these molecules on the outside surface of the micelles has created an environment in which FDA comes into contact with the histidine residues which achieves higher reaction rate. It is highly possible that the histidine molecules are coming in contact with one another, assisting in the transfer of the acetyl group and ultimately causing deacylation and turnover. Although cysteine has the capability of carrying out nucleophilic attacks with its thiol anion, they cannot produce turnover as the acetyl group stays on the thiol without the assistance of histidine removing the acetyl group. The combination of Peptides 20 and 21 shows slight decrease compared to Peptide 20 on its own. A possible explanation of this phenomenon may be that Peptide 21 is over crowding the micelle surface and preventing the histidine on Peptide 20 from freely reacting with FDA. Peptide 22 also shows increase in acetylation rate of FDA due to its presence of histidine on the outside of the micelle surface unlike Peptide 23 which brings the cysteine residue at the closest proximity to FDA molecules. These results once again show the importance of having a structure that can bring the substrate and the peptide molecules closer to one another. Peptides 24 and 25 also enhanced the acetylation rate greatly due to their amidation on the c-terminal. It should be noted that the addition of Triton X-100 did not enhance the FDA hydrolysis rate for both peptides. This may be due to Peptides 24 and 25 already forming a micelle due to its increased hydrophilicity due to the amine termination which lowers its critical micelle concentration.

The results shown in Figure 36 indicate that these previous rates are highly dependent on the concentration ratio between the substrate, peptides, and surfactant. It is ideal to have a high substrate to catalyst ratio in order to reduce cost. Also, it shows that

the fewer catalysts used to hydrolyze the substrate, the more efficient the catalysis can progress. In our second study, we have chosen the ratio 5:1 for the substrate to peptide. In this study, the reaction rates were closer to the measured rates with Peptides 1 through 6 with Peptide 21 containing cysteine showing a higher rate than Peptide 20. Due to the lack of histidines coming in contact with one another, there is far less deacylation happening from acetyl transfer between the multiple histidines. Between Peptides 22 and 23, a surprisingly large difference can be seen when Triton X-100 is added. Once again, the orientation of the Cys-His matters and having a histidine near the micelle surface is favorable. This is consistent with the previous higher peptide concentration results. Unfortunately, the amidation terminated Peptide 24 and 25 did not perform as well as they did at higher concentration. It is possible that these peptides did not reach the critical micelle concentration.

1.7.4 **Conclusion**

From these results, it can be concluded that adding the palmitoyl terminated peptides were successfully inserted in the existing micelle structures of Triton X-100. Although Triton X-100 increases the hydrolysis rate of FDA on its own, adding high concentrations of peptides in some cases helped to increase the original reaction rate by around 50 fold. The micellular structure is very effective in creating an environment in which the peptides can interact with each other in precise manner as seen with Peptide 20. However, at lower concentrations, this interaction becomes more difficult to achieve since each micelle contains very few peptides. Although the micelle surface has the catalytic groups present, the interaction between the peptides are not enough to carry out

the catalysis as we hoped to see. It will be interesting to find a balance between a certain concentration of micelle, substrate, and peptide that can perform effectively enough to produce turnover at a cost effective manner.

1.8 Micelles with Electric Field

In the previous studies, we aimed to see the effect of the micelle structures created by Triton X-100 that helped direct the peptides in which the catalytic amino acid groups were directly in contact with the substrates at the micelle surface. In this section, we would like to focus on the peptides themselves forming a micelle and the addition of applied electric field. As shown in Figure 34, we attempted to achieve catalysis within micelles by pulsating the positively charged acetyl-histidine and the free thiol anion to avoid the back-attack from the thiol.

1.8.1 Experimental Methods

Unlike the previous electric field studies with homogeneous peptide catalysis which utilized UV-Vis cuvettes as the electric field fluidic chamber, fluidic chambers which consisted of two gold slides facing each other with 1 mm thick acrylic opening in between were used. 600 μL of sample fluid was contained in a laser-cut acrylic fluidic chamber. The gold slides were made in the cleanroom of UCSD Nano3 by using an E-beam evaporator and applying 10 nm and 200 nm of Ti/Au layers. This allows for controlled electric field to be applied consistently. The setup of the gold slide is shown in Figure 37. Previously mentioned Peptides 20 through 25 were reacted at 0.05 mM with 0.01 mM FDA in 0.1x TB pH 8.5 in the 600 μL fluidic chamber at room temperature. There was no Triton X-100 present in order to study the capability of peptides creating

micelles by themselves. The fluorescence measurements were only taken once at the 30 minutes time point since the solution cannot be removed readily from the fluidic chamber while the reaction progressed. Initially, all peptides were studied under zero voltage condition; however, in the second set of experiments where electric field was applied, only Peptide 25 was used since it showed the greatest promise from the previous micelle results. Square waves and pulsed electric field were tested at various voltage, frequency, and duty cycle.

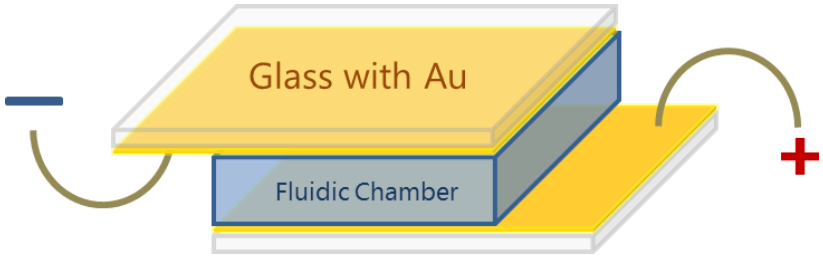

Figure 37: Fluidic chamber with gold on top and bottom surface.

1.8.2 **Results**

Figure 38 shows the initial results without the applied electric field. Although Peptides 20, 22, 24, and 25 showed statistically significant increase, these rates are not exceptional with only two fold increase by the addition of Peptide 24. These increases can be attributed to similar reasons as previously mentioned. Peptides 20 and 22 allow micelles to form with interacting histidine molecules and Peptide 24 and 25 have strong interaction with FDA with their amidation on the c-terminal. Figure 39 shows our initial attempt at applying a square wave electric field on Peptide 25. A square wave of 20 Vpp was applied to 0.05 mM Peptide 25 and 0.01 mM FDA at 10 kHz, 100 kHz, and 1 MHz. At 10 kHz and 1 MHz, roughly twice the amount of FDA was hydrolyzed when the electric field was applied with Peptide 25. Although these increases may indicate that the

electric field is catching the moment when acetyl group is transferred to the histidine, we must proceed with caution since there can be many possible reasons that the electric field can increase the hydrolysis rate of FDA.

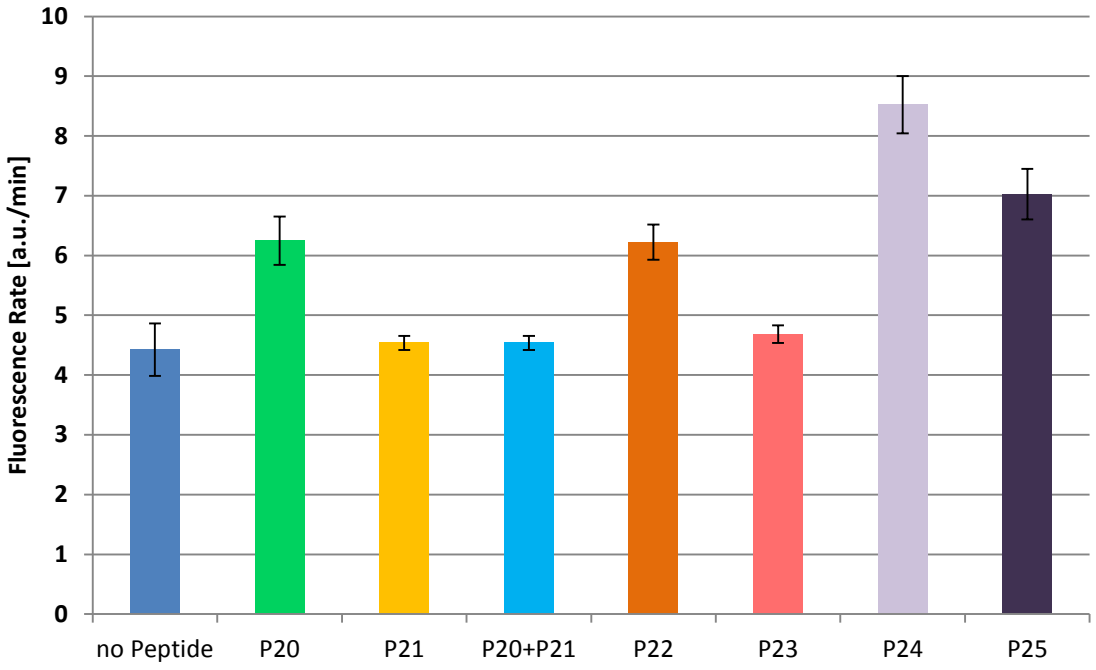

Figure 38: 0.05 mM of Peptide 20 through 25 reacted with 0.01 mM FDA without Triton X-100.

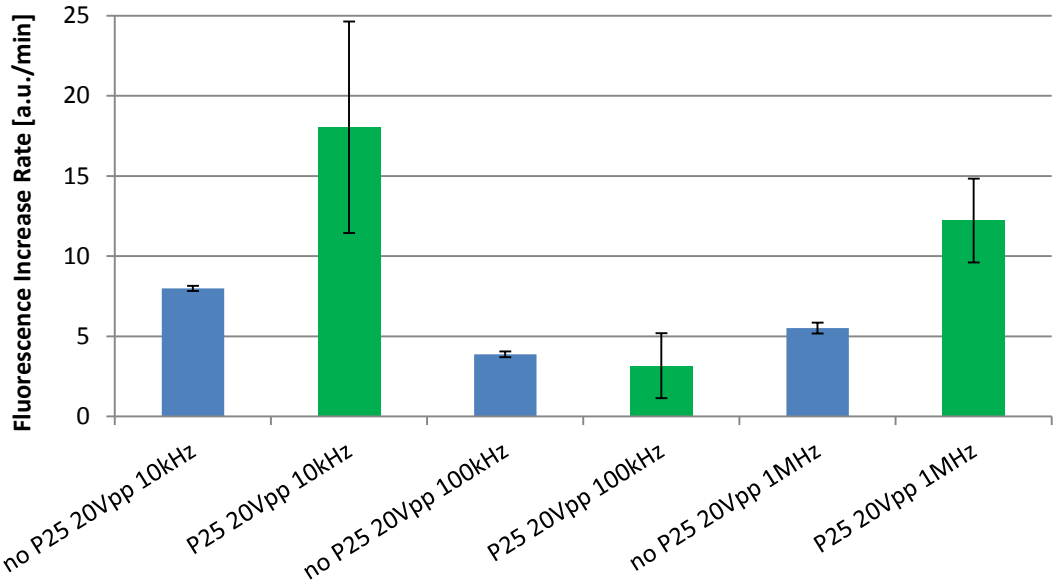

Figure 39: 0.05 mM Peptide 25 reacting with 0.01 mM FDA at 20 Vpp, 10 kHz, 100 kHz, and 1 MHz.

Upon rerunning Peptide 25 at 10 kHz 20 Vpp, the temperature before and after the reaction were measured. During this experiment, we noticed a slight increase in temperature. After running the experiment three times, the average temperature difference before and after was 1.1±0.1 °C. Since substrate hydrolysis rate dramatically increases with increase in temperature, we were unable to distinguish if this temperature rise had caused the rate increase or not. Furthermore, we tested 0.01 mM of FDA with 20 Vpp 1 kHz applied with and without 0.05 mM Peptide 25. Figure 40 shows that although there were dramatic increase on fluorescence rate, the absence and the presence of the peptide had little effect. Instead, the rate increase was due to the roughly 5 °C increase during the reaction. Although the overall average value is slightly higher for the reaction

that included Peptide 25, there is no statistical significance due to the error.

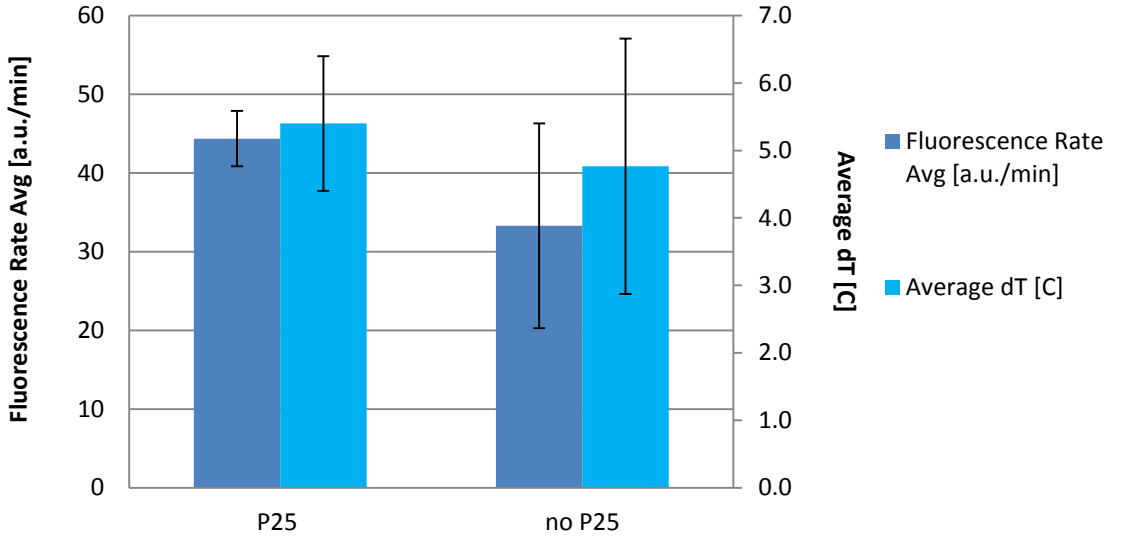

Figure 40: Fluorescence rate average (dark blue) and average change in temperature (light blue) of 0.01 mM FDA with 20 Vpp 1 kHz applied with and without Peptide 25.

1.8.3 Discussion & Conclusion

In this experiment, micelles were combined with electric field for the first attempt to utilize its charge difference of the acetyl-histidine and the thiol anion. However, the results showed little to no effect of electric field to achieve deacylation. Instead, at lower frequencies, increase in temperature was noticed, which caused the FDA to hydrolyze on its own. Although the effect of peptides themselves forming micelles was seen, none of the peptide showed exceptional increase in hydrolysis rate without the aid of Triton X-100. In order to avoid joule heating and to see the actual effect of electric field on the peptides, lower voltage at higher frequency must be applied. The current function generator can only produce up to 10 MHz; however, if pulsed electric field was used instead of square wave, there may have been more impact on the reaction since pulses can be produced shorter time frame (~40 ns) to catch the peptides during the acetyl-

histidine state. In our future work, it is important to focus on the actual mechanism of the peptide movement within the micelle and understand how each strand of peptide is moving during each electric field pulse. This may be accomplished by dynamic simulation which can take into account charges affected by applied electric field.

1.9 Gold and Polystyrene Nanoparticles

Another method to stabilize the peptide molecules is by attaching one or more ends of the peptide chain to a surface. In our studies, gold nanoparticles were functionalized with alkane thiol chains in order to perform a reduction reaction that attaches the peptides to the surface through the lysine secondary amine. Gold surface was chosen due to its relatively high density of possible thiol reaction which allows large numbers of peptides present on each nanoparticle. In addition, gold nanoparticles can be synthesized in various sizes from 5 nm to 40 nm diameters in relatively simple procedures. Smaller diameter gold nanoparticles have larger surface to volume ratio, which allows greater reaction of substrate to peptide; however, small nano particle (< 10nm) are difficult to keep suspended in various mediums and after various washing steps required to achieve the final peptide functionalization(47, 61, 71-75).

Polystyrene nanoparticles were also used in conjunction with biotin-streptavidin linkers for the peptides. Biotin-streptavidin is one of the strongest bonds available in organic molecules that do not require covalent bonds; therefore, simple conjugation of peptides can be achieved with high specificity and yield. The polystyrene beads came pre-functionalized with a known concentration of streptavidin. Our peptides were modified to have biotin attached on the n-terminal of the peptides. Upon functionalizing

the gold and polystyrene nanoparticles, they were once again tested with substrates FDA, and 4-methylumbelliferyl butyrate (MUBB) for esterase activity.

1.9.1 **Experimental Methods**

100 mL of 10-12 nm gold nanoparticles were synthesized using the following methods.

Two solutions were made: Solution A) 79 mL DI water with 1 % w/v aqueous gold chloride and solution B) 4 mL 1 %w/v trisodium citrate, 25 μL 1 % w/v tannic acid, and 16 mL DI water. The two solutions were heated to 60 °C and mixed while stirring. When the color turned to dark shade of red, the solution was heated up to 95 °C for one minute and then cooled on ice. The gold nanoparticles were centrifuged at ~9000 xg for 30 minutes to remove the supernatant and suspended in ethanol for the following procedure. After the synthesis, the particles were observed under scanning electron microscope (SEM) and the particle sizes were measured with UV-Vis and dynamic light scattering (DLS) to confirm the diameter of around 10-12 nm.

1 mL of the synthesized gold nanoparticles were centrifuged for 20 min at 1600 xg and resuspended in 50 uL of 5 mM 11-mercaptoundecanoic acid (MUA) in ethanol for at least 24 hours. The particles were spun down again for 20 minutes at 1600 xg and resuspended in 400 μL MES buffer. 50 μL of 2 mM 1-ethyl-3-[3-dimethylaminopropyl] carbodiimide (EDC) was added to the MES buffer and sonicated for 15 minutes. 50 μL of 5 mM N-hydroxysulfosuccinimide (NHSS) was added to the MES buffer and sonicated until fully dissolved and reacted for 15 minutes. 1 μL of 2-mercaptoethanol was added to quench the EDC activation reaction. Finally, 100 μL of 2 mM lysine terminated Peptide

14 was added and reacted for 2 hours. The solution was centrifuged for 20 minutes at 1600 xg and resuspended in 60 µL DI water. The previous steps were repeated until enough volume of solutions was obtained. Figure 41 shows the order of the functionalization.

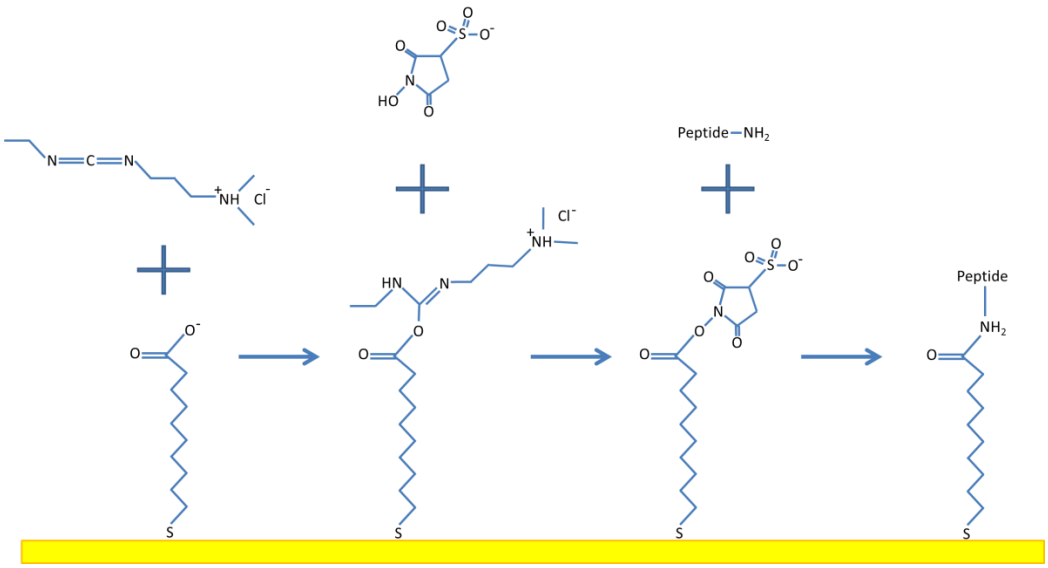

Figure 41: Thiol-alkane functionalization using EDC, NHSS, and amine terminated peptide.

0.01 mM FDA was reacted with the Peptide 14 functionalized gold nanoparticle in the 600 µL cuvette. In addition, same reaction was tested in the z-dimensional gold electrode fluidic chamber at 200 µL of total volume. LS 50 Perkin Elmer Fluorometer was used to measure the activity of FDA with 390 nm/515 nm for excitation and emission spectrum. The controls included FDA, FDA with non-functionalized gold nanoparticle, and FDA with thiol-alkane functionalized gold nanoparticles. 20 Vpp 10 MHz were applied to see the effect of electric field on the peptides.

Four biotin terminated peptides were designed to react with 110 nm diameter streptavidin coated beads (Bangs Laboratories, Inc.). Peptides 26 and 27 contained biotin at the n-terminal and one residue of histidine and cysteine respectively. Peptide 28

contained biotin-Cys-Phe-His and Peptide 29 in reverse order, biotin-His-Phe-Cys. Due to the limited availability of the streptavidin coated nanoparticles, only Peptide 28 was tested since it had the histidine on the c-terminus, which has proven to be effective in the previous micelle experiments.

Initially, Peptide 28 was dissolved in excess amount directly into 200 μL streptavidin bead solution and reacted for 2 hours. The beads were centrifuged in a mini Eppendorf centrifuge for 10 minutes to remove the excess peptide. After the final wash, the beads were resuspended in 0.1x TB pH 8.5 buffer solution. Upon calculating the actual concentration of peptide in the solution, we learned that there was only 4.4 μM of Peptide 28 even after ten times dilution. We decided to attempt to increase the concentration of the beads using less fluid during resuspention. Initially, 800 μL of beads were reacted with excess amount of Peptide 28. After the second attempt of dilution, wash, and resuspention, we attained 22 μM Peptide 28 on the surface of the beads. These beads were then reacted with 0.5 mM MUBB for 30 minutes with 10 Vpp 10 kHz and 20 Vpp 10 kHz applied throughout the reaction. The controls include MUBB, MUBB with bead buffer which consists of 0.1 M MES + 0.1 % BSA + 0.05 % Tween 20 + 10 mM EDTA, MUBB and streptavidin coated beads, and MUBB with Peptide 28.

1.9.2 **Results**

Figure 42 shows the results from 0.01 mM FDA reacted with gold nanoparticle functionalized with Peptide 14. There is a clear increase in fluorescence rate once the substrate is reacted to the peptide attached to the gold nanoparticle. There is a noticeable increase in the rate once the MUA is attached to the gold nanoparticle. This may be due

to the carboxylic acid slightly reacting with the substrate or free thiol-alkane molecules in the solution. Figure 43 shows the reaction rates with applied electric field for the peptide functionalized gold nanoparticles. This plot shows contradictory results from Figure 42 since it shows that Peptide 14 actually has an adverse effect. Once 20 Vpp 10 MHz was applied, the reaction rate actually decreased. The controls that contained the thiol alkane chain on the gold nano particle surface showed a slight increase in rate. This may be due to the charged carboxylic acid at the end of the alkane chain which is slightly reactive compared to the bare gold surface.

Figure 44 shows the 0.5 mM MUBB reacted with streptavidin bead and Peptide 28. Clear increase can be seen once the Peptide 28 is attached to the streptavidin coated beads. When the electric field is applied, there was an increase in hydrolysis rate when 20 Vpp 10 kHz was applied, but not 10 Vpp 10 kHz.

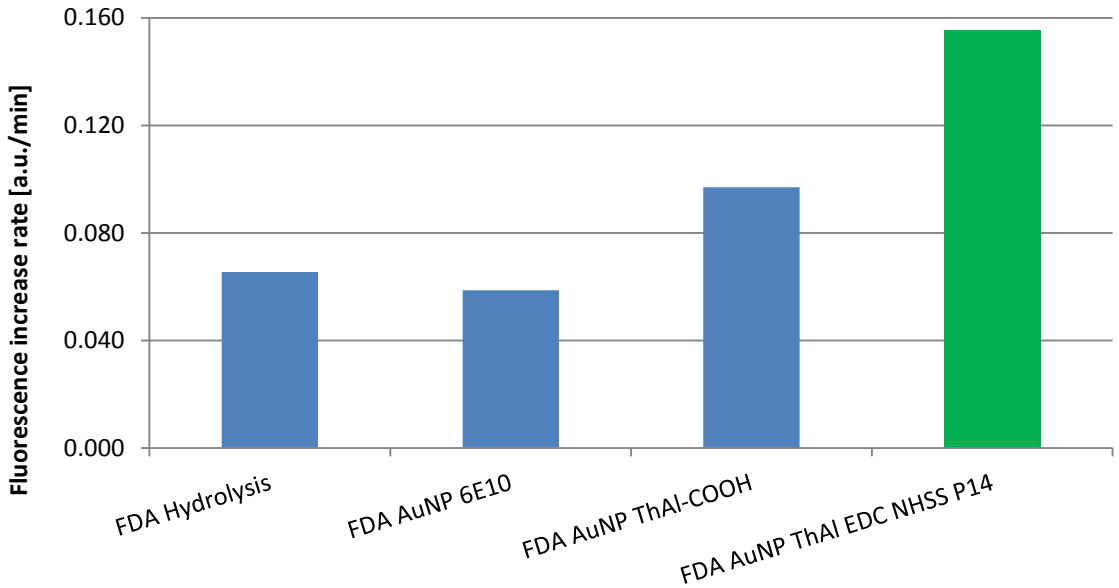

Figure 42: 0.01 mM FDA reaction rate with 10nm gold nanoparticle attached to Peptide 14 in 600uL cuvette.

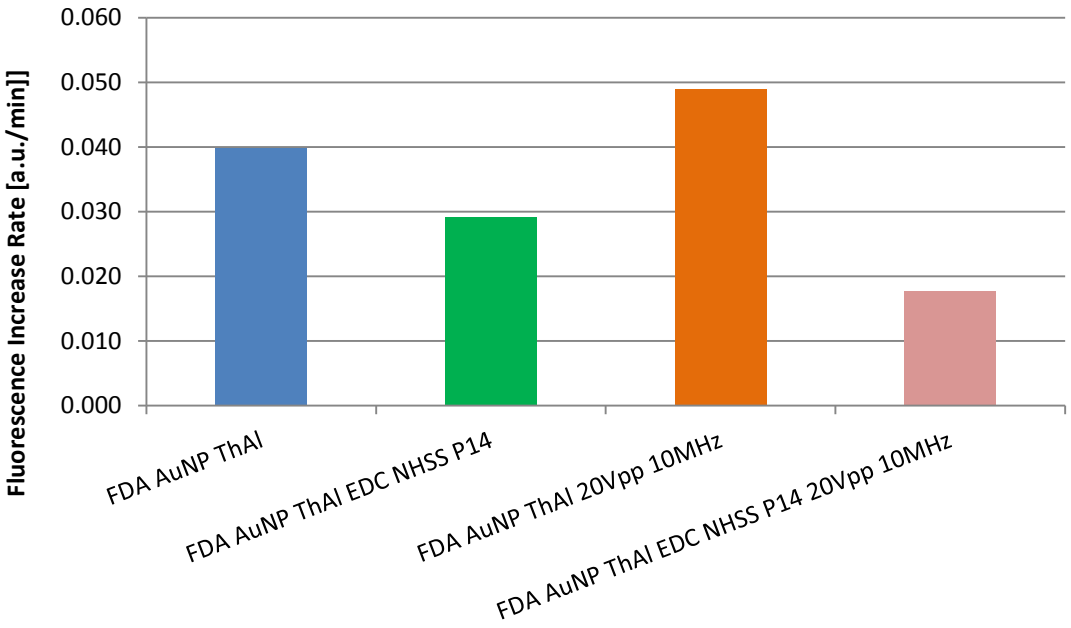

Figure 43: 0.01 mM FDA reaction rate with 10nm gold nanoparticle attached to Peptide 14 with applied electric field in 200uL cuvette.

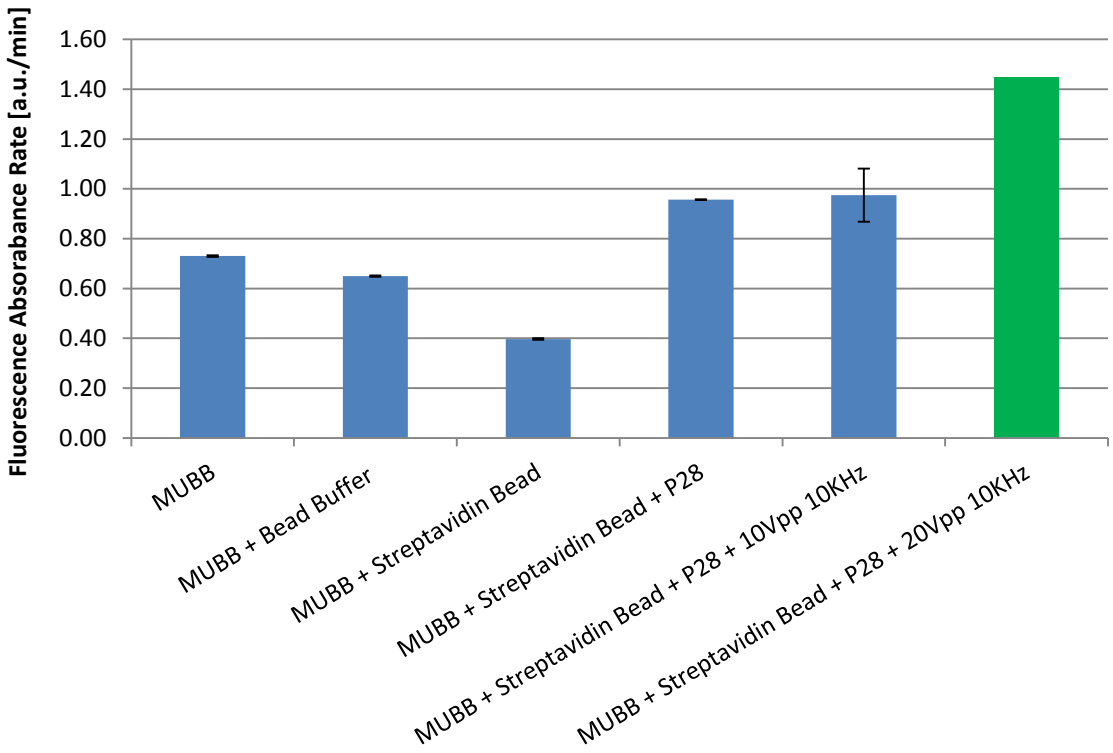

Figure 44: 0.5 mM MUBB reacted with Peptide 28 functionalized polystyrene nanoparticles and 20 Vpp 10 kHz applied.

1.9.3 Discussion and Conclusion

Throughout the gold nanoparticle and polystyrene bead experiments, it was critical to measure the actual concentration of the peptide molecules present on the surface of the particles. Unlike homogeneous reaction and micelles, there is a strict limit to how much peptide can exist in the solution at one time. Although the particles were suspended and resuspended at higher density towards the end of the functionalization, we noticed limits at how concentrated the beads can be before they aggregated out of the solution. From the UV-Vis absorbance values of known gold nanoparticle solution and our synthesized nanoparticle solution, we estimated that 6E12 gold nanoparticles were used for the final reaction. This calculated number of particles does not take in the effect

of losing any particles during each of the washing and resuspention, which is highly likely to occur. For the total number of particles, with a generous estimate of covering the entire beads with packed alkane thiol groups, we still only achieve 15 μM of Peptide 14 on the total surface of the particles. In our previous micelle studies, we showed studies that used peptide concentration at 2 μM and achieved disappointing results without the aid the Triton X-100.

For the streptavidin coated beads, the original solution contained far fewer streptavidin binding sites than expected. For every bead, biotin binding capacity was calculated to be 4.38 μM in the original buffer. In our experiment, we were able to concentrate the beads at five times the original bead concentration before the beads started to aggregate. This concentration effect only achieved a final Peptide 28 concentration of roughly 22 μM in the solution. Once again, this is a generous estimate of the actual peptide concentration and realistically there is probably an order of magnitude fewer peptides that actually bonded with the beads. In addition, the streptavidin beads had a poor surface to volume ratio with its diameter of 110 nm.

In order to account for these low concentrations of the peptide, several adjustments must be made. The particles must be suspended in a medium which can handle very high concentration of the peptide coated nanoparticles as well as the substrates. Initially, the experiments focused on nanoparticles on the order of 10 nm diameter since more peptides would be aligned with the z-dimensional electric field within a limited volume compared to larger particles which would have peptides attached to the side of the nanoparticle. In the same volume, smaller nanoparticles can occupy more spaces, indicating that smaller volume to surface ratio is ideal. However, small

diameter nanoparticles contain large amounts of space in between each nanoparticle where substrates do not come into contact with the nanoparticle. In our future studies, we would like to focus on using larger particles that can fill the empty volume within the solution, allowing greater nanoparticle surface to substrate interaction. This concept is similar to using a bead column for purification which involves particles getting imbedded or in contact with numbers of beads. In the concluding chapter, we will discuss other concepts of electric field induced catalysis and the use of nanoparticles in order to produce turnover.

1.10 Peptide on Gold Surface

In the previous two studies which incorporated peptides with micelles and gold nanoparticles, one of the major flaws was the misalignment of the majority of the peptides against the applied electric field. While the peptides were inside of the micelles or attached to the nanoparticles, majority of the peptides were misaligned against the vertical electric field that was applied due to micelles and nanoparticles being circular and electric field being one dimensional. Although consistent electric field was applied to all particles, peptides that faced 90 degrees from the electric field would have no positive effect due to the misalignment of the charges. Therefore, only a small portion of the entire peptide concentration would have experienced the effect that we hoped to see in Figure 26.

In order to solve this problem, we attached the peptides directly onto the surface of the gold electrodes. Peptides that contained a lysine at the n-terminal can be attached to the gold surface similarly to those on the gold nanoparticles. In addition, Peptides 15,

17, and 19 contains aspartic acid groups at the c-terminal. The negative charge on the aspartic acid allows the entire peptide chain to be pulled when a positive bias is applied to the electrodes. As previously seen from the NAMD and VMD simulation, we have found that the peptide chains with higher rigidity makes the Cys-His bond distance variation to become smaller, in return allowing higher rate of acetyl exchange between the two amino acids. The electric field pulling on the aspartic acid will straighten the peptide chains by applying force on the negative charge. Although this method achieves great control over the peptide chain structure, the main drawback is the low interrogation volume of the solution. Since the peptides are attached to the surface, the overall charge of the substrate must be either positively charged or very close to neutral and must be contained in a very thin z-dimension to decrease uninterrogated substrates. If the molecules never touch the surface of the gold slide, the peptides will never react with the substrates. Thinner fluidic chamber allows the substrates to diffuse towards the surface.

1.10.1 **Experimental Methods**

Both horizontal and vertical directions of the electric field were applied using two different layouts of the gold slide (Figure 45). Interweaving lines of gold electrodes (10 nm Ti/100 nm Au) were made by standard photolithography method in the UCSD Nano3 Cleanroom. As shown in Figure 46, the lines were 50 μm thick in width and 50 μm apart from each other. It is important to mention that although the electric field was applied in a seemingly horizontal manner, the produced electric field were more vertical at the center of the electrode lines, meaning that the peptides would have electric field applied

perpendicular to the electrode surface. This would cause the peptides to be pulled away from the electrode surface as expected.

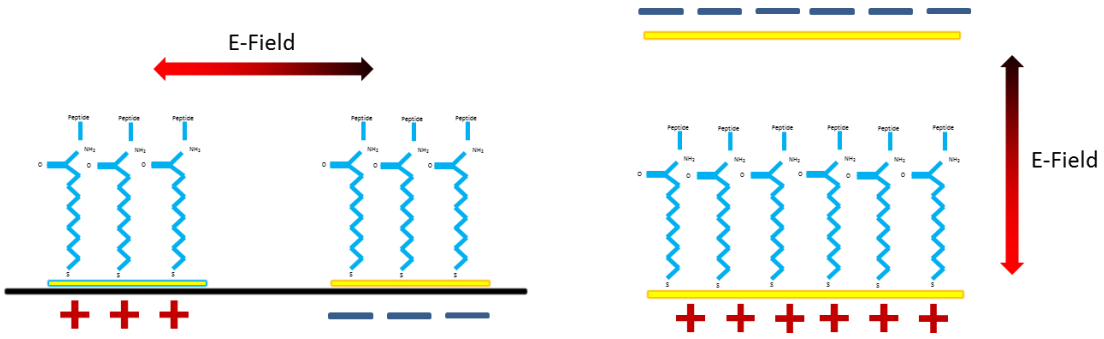

Figure 45: Scheme of electric field perturbation in (left) horizontal and (right) vertical electric field.

Figure 46: (left) CAD diagram of the interweaving 50um thick gold electrodes. Electrodes images under a fluorescence microscope (center) before and (right) after functionalization of BODIPY die to confirm MUA-EDC-NHSS-Lys-Peptide bond. Each gold lines are 50 µm in width.

Peptide 14 was functionalized by using EDC-NHSS reduction from MUA attached to the gold slide. Initially, 1" x 3" gold slides were cleaned with acetone, ethanol, DI water and dried with nitrogen air. The slides were functionalized with 0.5 mM MUA in ethanol for 24 hours. The surface was then rinsed with ethanol for 10-15 seconds, dried and sonicated for 3 minutes. The previous step was repeated three times. The slides were placed in a plate with 50 mL of 0.1 M MES 0.5 M NaCl buffer pH 6 and 47.9 mg (10 mM) of EDC was added and sonicated for 15 minutes. 14.4 mg (5 mM) NHS was then added to the same plate, sonicated until everything was dissolved, and reacted for 15 minutes. The slides were rinsed with DI water and dried for further functionalization with

the peptides. Peptide 6 was used for the interweaving electrode setup and Peptide 14 was used for the vertical electric field setup. About 100 μL of 1 mM Peptides 6 and 14 were dissolved in DI water. 25 μL of peptide were added to the slide and glass slide was placed on top to spread the solution. After 2 hours of reaction, the slides were rinsed with DI water and dried.

The deacylation experiments with Ellman's reagent were carried out with the Peptide 6 functionalized interweaving electrodes. A 1 mm acrylic fluidic chamber was used with an acrylic cover on top to hold 150 μL of the sample. 0.9 μL of acetic anhydride was added in 599 μL of 0.05 M borate 0.1 M NaCl buffer pH 9.5 of which 150 μL was added to the fluidic chamber to prepare for the initial acetylation of the peptides. After 30 minutes, the fluid was removed from the fluidic chamber and exchanged with 150 μL of Ellman's reagent. The cathode and the anode of the electrodes were then connected to a function generator and applied 10 Vpp 10 MHz and reacted for 3 hours and 23 hours. Once the reaction was finished, the fluid was taken out and diluted in 450 μL of Ellman's reagent to have total volume of 600 μL. Controls for this experiment included functionalized gold slides without applied electric field.

For Peptide 19, vertical electric field was applied to the electric field by placing the sample fluid in between two gold slides without a fluidic chamber to reduce the gold-gold distance to minimum amount. Peptide 19 was functionalized to the bottom gold slide similarly to Peptide 6 with 11-mercaptoundecanoic acid-EDC-NHSS reduction. The thiol-alkane reaction was preceded for 48 hours instead of the previous 24 hours for Peptide 6 functionalization.

Once the functionalization was completed, acetylation reaction with 0.05mM MUBB was tested in 0.1x TB pH 8.5 at room temperature. In order to minimize the uninterrogated volume of sample, there was no fluid chamber used and instead, the gold slides were simply placed on top of each other with the 20 μL of sample fluid in between. This created a 1" x 1" square chamber in which the sample fluid was free to expand. Knowing the initial sample volume and the surface area, the height of the fluid was estimated to be roughly 10-20 μm. Once the fluid was properly set, 10 mV DC or 20 mV pulse at 50 % duty cycle was applied and the reaction was continued for 30 minutes. The reaction was terminated by removing 2 μL of the sample from the slides and diluting it 1:10 in DMSO. The products were measured in Tecan Fluorometer with Infinite 200 PRO NanoQuant plate which requires 2 μL of each diluted sample.

1.10.2 **Results**

The results for Peptide 6 on the interweaving electrodes are shown in Figure 47. From 3 hours to 23 hours, there is little difference seen that suggests that there was any increase in reaction with the electric field. The initial 23 hour run with electric field showed a substantial increase; however, this results could not be repeated for any other day (12/8, 12/10, and 12/11 denotes dates of the experiment).

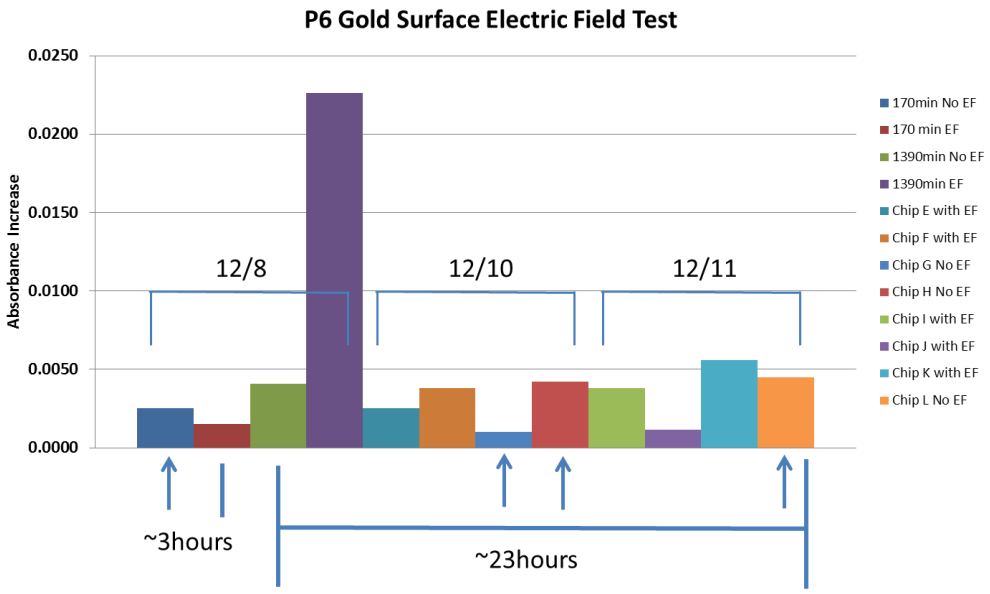

Figure 47: Peptide 6 gold surface electric field rates.

Figure 48 shows the results of fluorescence increase from the acetylation of 0.05 mM MUBB in the vertical gold slide device which the bottom slide was conjugated with Peptide 19 (Ac-Lys-Gly-Phe-Cys-Phe-His-Phe-Asp).

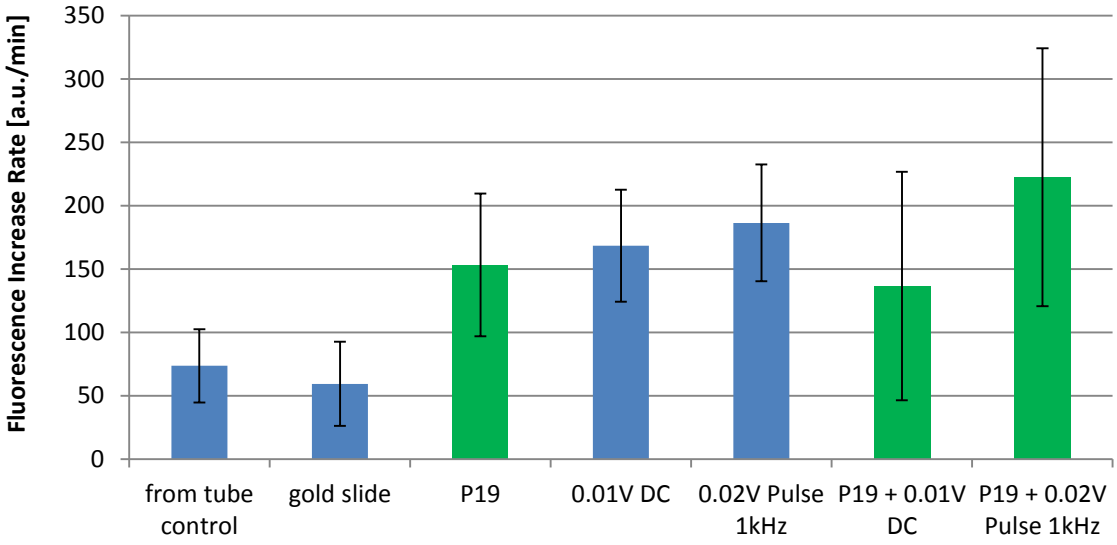

Figure 48: Rate of fluorescence increase from 0.05 mM MUBB reacted in vertical electric field gold slide device.

The first control involved taking 2 μL of the reaction sample from the tube and diluting it with DMSO. The second control involved taking 2 μL of the reaction sample from the gold slide device which has no peptide conjugated to the bottom gold slide. Each electric field setting was tested in conjunction with gold slide with and without Peptide 19 conjugation. The Peptide 19 conjugated gold slide showed over two times the average reaction rate compared to the two controls. This result clearly shows that the substrate is coming into contact with the peptide on the surface and acetylating which confirms that the method was successful. Upon applying the two forms of electric field, 10 mV DC and 20 mV pulse 1 kHz at 50 % duty cycle, there was no significant difference seen with gold slides with and without Peptide 19 conjugated. Noticeable evaporation was also seen from devices with applied electric field, indicating the possible increase in the temperature which would be detrimental to the rate constant measurements. Due to the small volume between the gold slides (20 μL), we were only able to obtain 2 μL with decent consistency. Several measurements were omitted due to the lack of sufficient sample removal due to evaporation. These errors have contributed significantly and can be seen with the large error bars especially for the Peptide 19 combined with the two forms of electric field. Although the application of electric field showed inconsistent and insignificant results, the overall experiment showed promise in conjugated peptide surfaces by proving that the platform in which low volume/large surface area devices can be used to create an environment in which substrate to peptide contact is increased. In the future, any lysine terminated peptides can be used to be conjugated on a gold surface using a similar experimental design.

4

Conclusion

1.11 Homogeneous Peptide Catalysis

Catalysis using nanostructures have been investigated for decades and some have started to claim that they are producing real turnover with purely synthetic chemistry. However, there is a clear lack in effort in replicating the truly mechanical nature of the enzymes. In our studies, we designed and tested a series of peptides in which contained the catalytic group of cysteine protease, papain. We have successfully demonstrated that not only the distances between the two catalytic amino acids, but the movements they make are critical in terms of transferring the acetyl group cleaved from the substrate. The minute change in the dynamic motion created by the peptide backbone has significant impact towards the acetyl group transfer rate between the cysteine and the histidine. From the studies of Peptides 14 through 19, it has shown that there is little effect of the aspartic acid group which is the third member of the catalytic triad. However, by adjusting the length of the peptides, we were once again able to confirm the importance of the motion of Cys-His interaction. Throughout these studies, molecular modelling simulation has

shown promising results by measuring the distances between the two residues and the end-to-end distance of each peptide throughout a certain time scale. In the future, we would like to continue to pursue designing the peptides through simulation in order to achieve a more solid backbone that allows greater interaction between the cysteine and the histidine.

1.12 Heterogeneous Peptide Catalysis

Although the homogeneous studies with peptides have shown great promise and provided us with insight towards the requirement of structural rigidity of the peptide design, the actual implementation of these structures is still very difficult. Also, in the homogeneous peptide studies, we have focused on producing a greater acetyl exchange rate between the two amino acids, but we have yet to discover a method that can efficiently bring the acetyl-histidine group further away from the cysteine to prevent back-attack. The electric field approach is a simple idea that takes advantage of the charge changing state during the interaction between the substrate and the peptide. The key issues that we faced were: 1) applying the electric field at the right moment when the acetyl group is on the histidine instead of the cysteine, 2) applying the electric field in the right direction or aligning the peptides with the electric field. The first issue is extremely difficult to tackle due to the difficulty of knowing how frequently and how long the acetyl group stays on the histidine before the cysteine attacks. Although we have performed Ellman's reagent tests, it does not provide an exact length of time in which each event to occur. Also, each peptide reacts at different time in a different space. Due to these variables, applying a single electric field pulse may have little effect on the

overall catalysis. A possible solution to this may be applying a constant positive bias DC electric field to align the peptides first and then applying an electrical pulse in addition to move the acetyl-histidine away from the thiol anion.

1.13 Future directions

1.13.1 Peptides

As explained previously, a highly rigid backbone of the overall peptide increases the interaction between the catalytic groups. This can be achieved in homogeneous solution by controlling the two ends of the peptides. We have plans on creating cyclic peptides that contain multiple cysteine histidine residues. By creating a closed loop of peptides, a highly stringent structure can be built. Several other techniques that can be used are attaching the catalytic groups to DNA hairpin structure or DNA origami.

Besides studying the effect of Ellman's reagent to measure the acetyl-transfer rates, we have searched for methods using a fluorescent thiol ester to see the acetyl group leaving in real time. By attaching a fluorescent thiol ester to a surface, fluorescent microscopy can be used to directly view the decrease in fluorescence once the fluorescent acetyl group deacylates from the thiol. Although catalytic rates can be measured through UV-Vis or fluorescence increase of the entire solution, due to our focus on measuring the rate of a single mechanism of the entire substrate cleavage process, a specific method for each reaction must be used. One problem while running these experiments is that, enzyme substrates are becoming increasingly difficult to find in general chemical catalogues due to the lack of popularity and increased focus towards general substrates.

Knowing these challenges, we have come to the conclusion that there are still vast arrangements that peptides can be designed to produce catalysis.

1.13.2 **Micelles & Nanoparticles**

Of course, synthetic enzymes in micellular environments can be combined with a variety of other formats, including devices that provide electrical fields or fluidized beds to provide further enhancement of reaction rates. Below, we describe several such formats.

We have recently started the study of synzymes that will mimic the behavior of desaturases. Although desaturase mimics will require different chemical structures, such synthetic enzymes can also be combined with micelles and devices that provide electrical fields or fluidized beds. We chose to model the active sites of soluble desaturases because of the availability of X-ray crystallographic data. Such active sites contain four glutamic residues and two histidines, which coordinate with two iron atoms(76, 77).

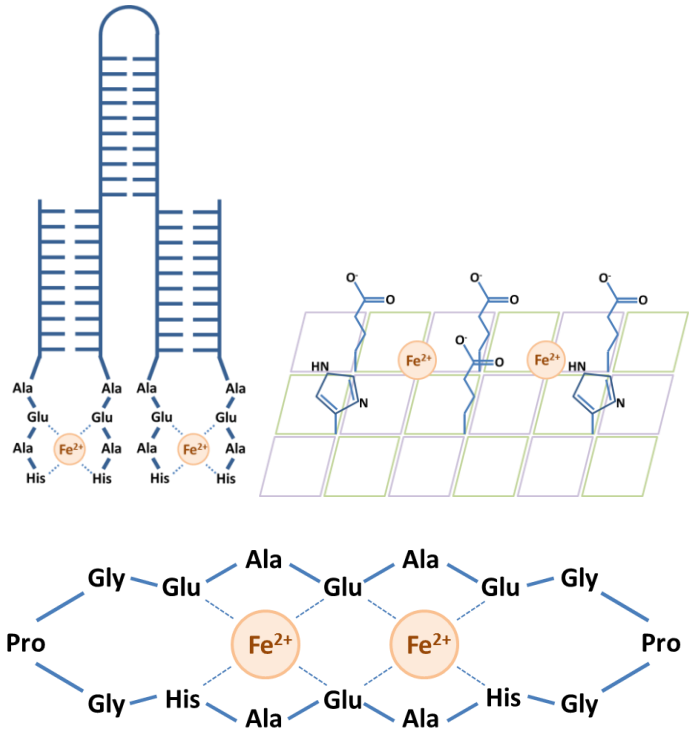

Figure 49: Desaturase Mimics: Two DNA/Peptide Structures with Diiron Sites Including a DNA Hairpin Structure, a DNA Origami Structure and a Cyclic Peptide with a Diiron Site.

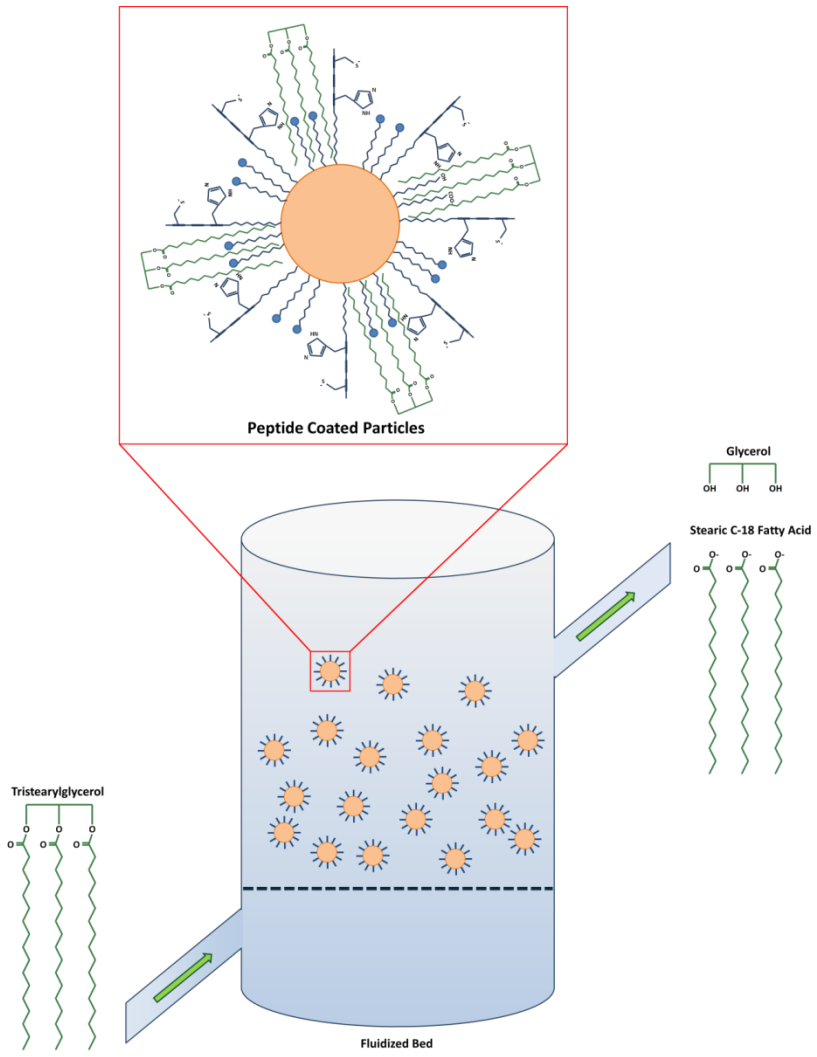

Figure 50: Fluidized Bed with Lipase Mimics Linked to Particles.

Figure 50 shows synthetic enzymes immobilized on particles can be used in a fluidized bed format. Here the synzymes are interspersed with amphiphilic polymers bound to the surface, which are shown in blue. Fluid circulation in the fluidized bed enhances the perceived reaction rate by moving the substrate near the synzymes on the particles. Products are removed through a membrane that blocks the escape of the particles.

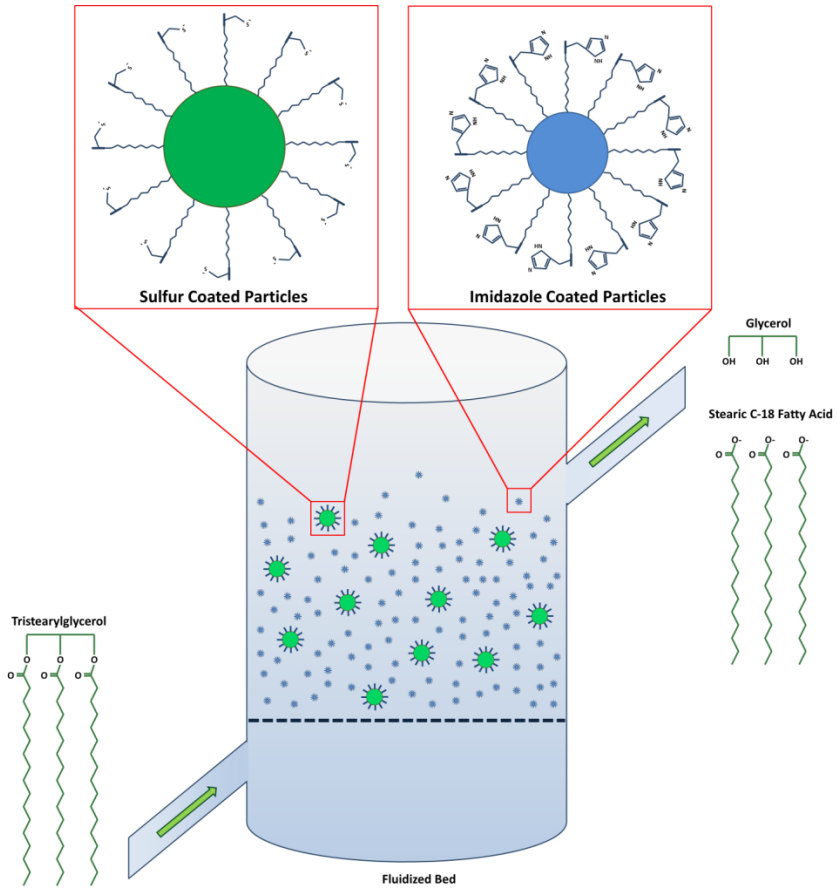

Figure 51: Fluidized Bed with Thiol/Imidazole Linked Particles.

We have also envisioned another fluidized bed format in which the sulfur and imidazole groups are on different particles. Here, the imidazole groups would be on smaller, more numerous beads beads because, otherwise, the more reactive sulfur would be likely to participate in a back attack on the acyl group, thus halting the reaction. Once again, the bead volume to surface area ratio must be considered with care in order to increase the substrate/thiol/histidine interactions.

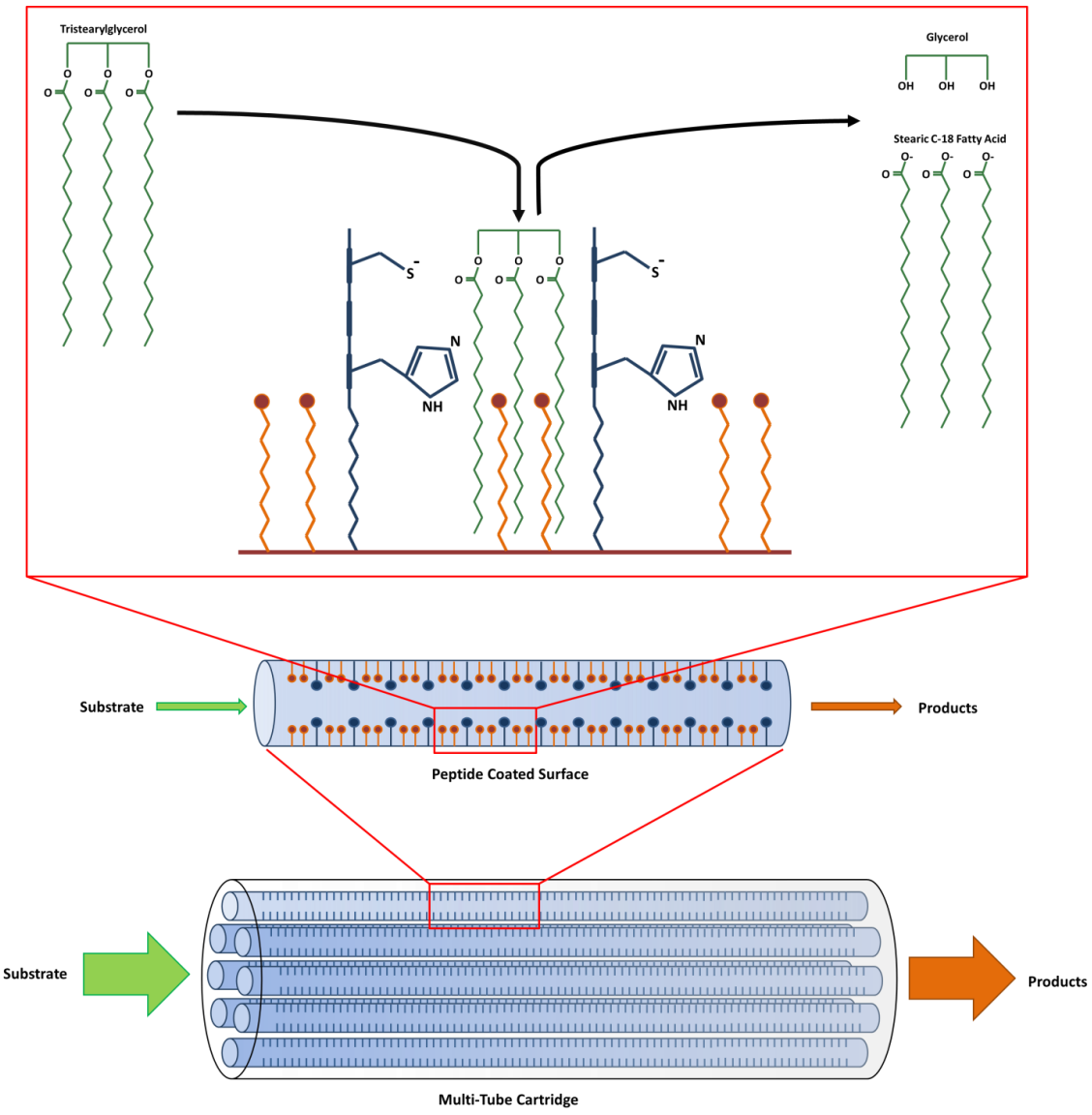

Figure 52: Lipase Mimic in a Flow-Through Device.

In Figure 52 synthetic enzymes are coated onto or covalently linked to the inner surfaces of the channels in the flow-through device or cartridge with a great amount of surface area provided by the channels. The synzymes can be interspersed with amphiphilic polymers composed hydrophobic linker groups with hydrophilic end groups, shown in red. Typically the end groups would be hydroxyls or other relatively non-reactive groups. The amphiphilic polymers provide a hydrophobic environment to attract

hydrophobic substrates. In addition, the amphiphilic polymers minimize crowding or steric interference between active sites. Such amphiphilic polymers can also be used to passivate the surfaces of the channels to prevent the active sites from sticking to the surfaces. The active sites are composed of cysteine and histidine residues with other amino acid residues between them to facilitate the correct orientation of the thiols and imidazoles. The fluid flow through the cartridge should increase the perceived rate of the reaction by bringing the substrate near the active sites and removing the products, which will prevent them from participating in back reactions.

1.13.3 **Electric Field**

Figure 53 shows another use of electric field by separating the thiol peptide and the substrate by a difference in charge. Within a imidazole coated capillary tube, substrates and Cys-Arg-Arg peptide can be reacted to achieve an acetyl-thiol-Arg-Arg chain. By flowing the reaction product over the histidine, the acetyl groups can be removed. Since the removed product will have a positive charge and the remaining Cys-Arg-Arg has a net positive charge, the applied electric field will remove the substrate products while capable of reusing the Cys-Arg-Arg chain for further reactions. Although these devices are not complex, they will require a complete knowledge of the current back-attack problems. Implementation of these techniques would be rather simple and will allow the technology to scale into producing a large volume of products.

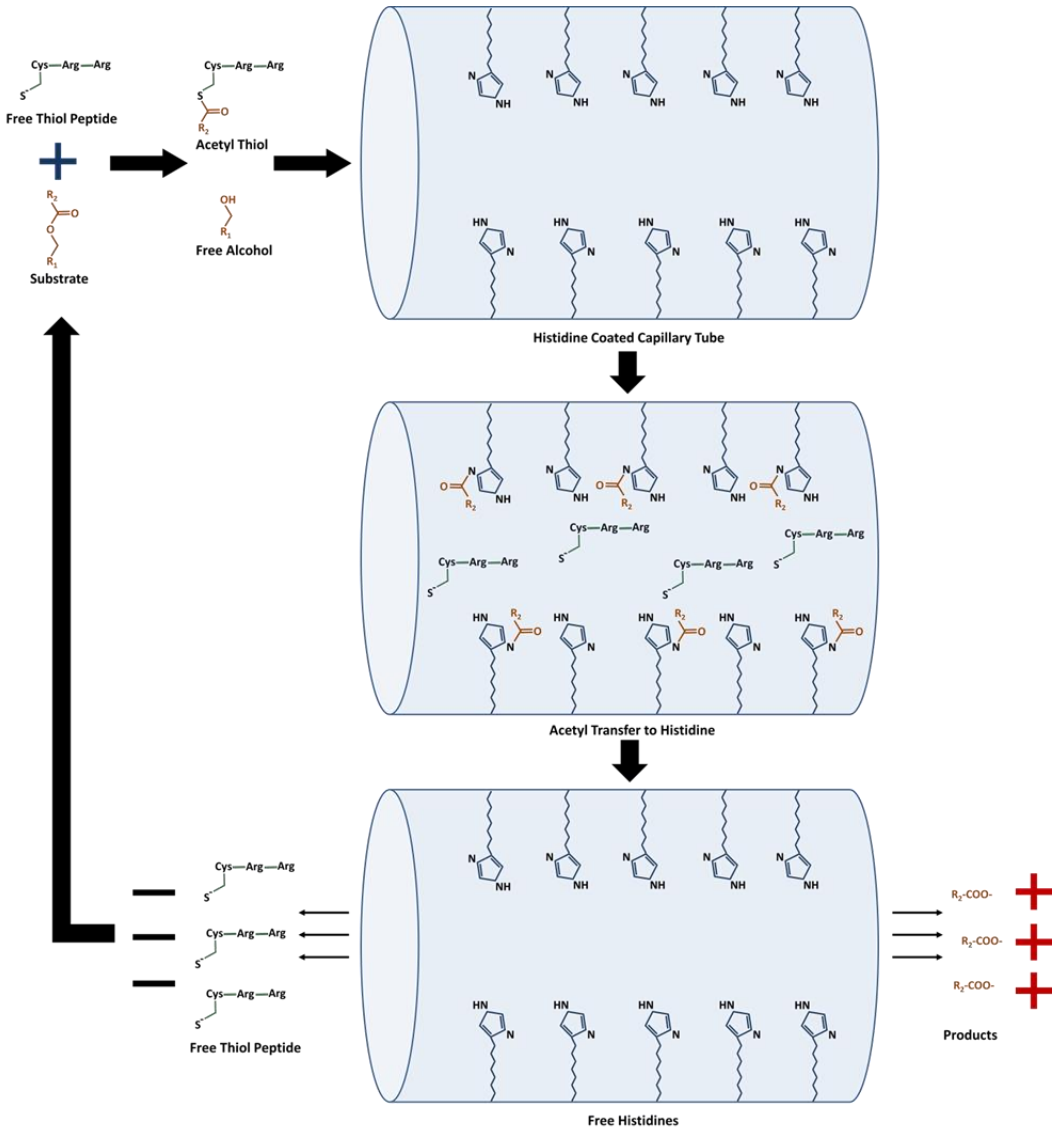

Figure 53: DC electric field induced flow through device. Histidine molecules are attached in the capillary tube while acetyl-thiol fragments are passed through the tube. Then, the DC charge will separate the free thiol and products due to their native charge.

5

References

1. Bjerre J, Rousseau C, Marinescu L, Bols M. Artificial enzymes, "chemzymes": current state and perspectives. Applied microbiology and biotechnology. 2008;81(1):1-11.

2. Breslow R. Artificial Enzymes. Artificial Enzymes: Wiley-VCH Verlag GmbH & Co. KGaA; 2006. p. 1-35.

3. Raynal M, Ballester P, Vidal-Ferran A, van Leeuwen PWNM. Supramolecular catalysis. Part 2: artificial enzyme mimics. Chemical Society reviews. 2014;43(5):1734-87.

4. Wei H, Wang E. Nanomaterials with enzyme-like characteristics (nanozymes): next-generation artificial enzymes. Chemical Society reviews. 2013;42(14):6060-93.

5. Aumuller T, Fandrich M. Protein chemistry: Catalytic amyloid fibrils. Nat Chem. 2014;6(4):273-4.

6. Berg JM. Zinc-finger proteins. Current opinion in structural biology. 1993;3(1):11-6.

7. Berg JM. Zinc Finger Domains: From Predictions to Design. Accounts of Chemical Research. 1995;28(1):14-9.

8. Bolon DN, Mayo SL. Enzyme-like proteins by computational design. Proceedings of the National Academy of Sciences of the United States of America. 2001;98(25):14274-9.

9. Corey DR, Phillips MA. Cyclic peptides as proteases: a reevaluation. Proceedings of the National Academy of Sciences of the United States of America. 1994;91(10):4106-9.

10. Corey MJ, Corey E. On the failure of de novo-designed peptides as biocatalysts. Proceedings of the National Academy of Sciences of the United States of America. 1996;93(21):11428-34.

11. Dong Z, Luo Q, Liu J. Artificial enzymes based on supramolecular scaffolds. Chemical Society reviews. 2012;41(23):7890-908.

12. Kisailus D, Truong Q, Amemiya Y, Weaver JC, Morse DE. Self-assembled bifunctional surface mimics an enzymatic and templating protein for the synthesis of a metal oxide semiconductor. Proceedings of the National Academy of Sciences of the United States of America. 2006;103(15):5652-7.

13. Kofoed J, Reymond JL. Dendrimers as artificial enzymes. Current opinion in chemical biology. 2005;9(6):656-64.

14. Korendovych IV, DeGrado WF. Catalytic efficiency of designed catalytic proteins. Current opinion in structural biology. 2014;27(0):113-21.

15. Rekharsky MV, Inoue Y. Complexation Thermodynamics of Cyclodextrins. Chem Rev. 1998;98(5):1875-918.

16. Rufo CM, Moroz YS, Moroz OV, Stöhr J, Smith TA, Hu X, et al. Short peptides self-assemble to produce catalytic amyloids. Nat Chem. 2014;6(4):303-9.

17. Wennemers H. Asymmetric catalysis with peptides. Chemical Communications. 2011;47(44):12036-41.

18. Wharton CW. Synthetic polymers as models for enzyme catalysis-a review. International Journal of Biological Macromolecules. 1979;1(1):3-16.

19. Chica RA, Doucet N, Pelletier JN. Semi-rational approaches to engineering enzyme activity: combining the benefits of directed evolution and rational design. Current opinion in biotechnology. 2005;16(4):378-84.

20. Dalby PA. Strategy and success for the directed evolution of enzymes. Current opinion in structural biology. 2011;21(4):473-80.

21. Gerlt JA, Babbitt PC. Enzyme (re)design: lessons from natural evolution and computation. Current opinion in chemical biology. 2009;13(1):10-8.

22. Kazlauskas R, Lutz S. Engineering enzymes by 'intelligent' design. Current opinion in chemical biology. 2009;13(1):1-2.

23. Pleiss J. Rational Design of Enzymes. Enzyme Catalysis in Organic Synthesis: Wiley-VCH Verlag GmbH & Co. KGaA; 2012. p. 89-117.

24. Tobin MB, Gustafsson C, Huisman GW. Directed evolution: the 'rational' basis for 'irrational' design. Current opinion in structural biology. 2000;10(4):421-7.

25. Beveridge AJ. A theoretical study of the active sites of papain and S195C rat trypsin: Implications for the low reactivity of mutant serine proteinases. Protein Science. 1996;5(7):1355-65.

26. Brocklehurst K, Malthouse JP, Shipton M. Evidence that binding to the s2-subsite of papain may be coupled with catalytically relevant structural change involving the cysteine-25-histidine-159 diad. Kinetics of the reaction of papain with a two-protonic-state reactivity probe containing a hydrophobic side chain. Biochem J. 1979;183(2):223-31.

27. Drenth J, Jansonius JN, Koekoek R, Swen HM, Wolthers BG. Structure of papain. Nature. 1968;218(5145):929-32.

28. Guthrie JP, Pike DC. Hydration of acylimidazoles: tetrahedral intermediates in acylimidazole hydrolysis and nucleophilic attack by imidazole on esters. The question of concerted mechanisms for acyl transfers. Canadian Journal of Chemistry. 1987;65(8):1951-69.

29. Harrison MJ, Burton NA, Hillier IH. Catalytic Mechanism of the Enzyme Papain: Predictions with a Hybrid Quantum Mechanical/Molecular Mechanical Potential. J Am Chem Soc. 1997;119(50):12285-91.

30. Heller MJ, Walder JA, Klotz IM. Intramolecular catalysis of acylation and deacylation in peptides containing cysteine and histidine. J Am Chem Soc. 1977;99(8):2780-5.

31. Houk KN, Leach AG, Kim SP, Zhang X. Binding Affinities of Host–Guest, Protein–Ligand, and Protein–Transition-State Complexes. Angewandte Chemie International Edition. 2003;42(40):4872-97.

32. Jencks WP. Mechanism of Enzyme Action. Annual review of biochemistry. 1963;32:639-76.

33. Lake AW, Lowe G. The kinetics of papain- and ficin-catalysed hydrolyses in the presence of alcohols. Biochem J. 1966;101(2):402-10.

34. Lecaille F, Kaleta J, Bromme D. Human and parasitic papain-like cysteine proteases: their role in physiology and pathology and recent developments in inhibitor design. Chem Rev. 2002;102(12):4459-88.

35. Otto H-H, Schirmeister T. Cysteine Proteases and Their Inhibitors. Chem Rev. 1997;97(1):133-72.

36. Tsukada H, Blow DM. Structure of alpha-chymotrypsin refined at 1.68 A resolution. Journal of molecular biology. 1985;184(4):703-11.

37. Takahashi T, Cheung M, Butterweck T, Schankweiler S, Heller MJ. Quest for a turnover mechanism in peptide-based enzyme mimics. Catalysis Communications. 2015;59(0):206-10.

38. Nemkevich A, Burgi H-B, Spackman MA, Corry B. Molecular dynamics simulations of structure and dynamics of organic molecular crystals. Physical Chemistry Chemical Physics. 2010;12(45):14916-29.

39. Fieser TM, Tainer JA, Geysen HM, Houghten RA, Lerner RA. Influence of protein flexibility and peptide conformation on reactivity of monoclonal anti-peptide antibodies with a protein alpha-helix. Proceedings of the National Academy of Sciences. 1987;84(23):8568-72.

40. Huang F, Nau WM. A Conformational Flexibility Scale for Amino Acids in Peptides. Angewandte Chemie International Edition. 2003;42(20):2269-72.

41. Pornsuwan S, Bird G, Schafmeister CE, Saxena S. Flexibility and Lengths of Bis-peptide Nanostructures by Electron Spin Resonance. J Am Chem Soc. 2006;128(12):3876-7.

42. Dunker AK, Lawson JD, Brown CJ, Williams RM, Romero P, Oh JS, et al. Intrinsically disordered protein. Journal of Molecular Graphics and Modelling. 2001;19(1):26-59.

43. Janin J, Sternberg MJE. Protein flexibility, not disorder, is intrinsic to molecular recognition. F1000 Biology Reports. 2013;5:2.

44. Mierke DF, Kurz M, Kessler H. Peptide flexibility and calculations of an ensemble of molecules. J Am Chem Soc. 1994;116(3):1042-9.

45. Wright PE, Dyson HJ. Intrinsically disordered proteins in cellular signalling and regulation. Nat Rev Mol Cell Biol. 2015;16(1):18-29.

46. Neumann E, Katchalsky A. Long-Lived Conformation Changes Induced by Electric Impulses in Biopolymers. Proceedings of the National Academy of Sciences of the United States of America. 1972;69(4):993-7.

47. Chen Y, Cruz-Chu ER, Woodard JC, Gartia MR, Schulten K, Liu L. Electrically Induced Conformational Change of Peptides on Metallic Nanosurfaces. ACS Nano. 2012;6(10):8847-56.

48. Bendicho Sl, Barbosa-Cánovas GV, Martín O. Milk processing by high intensity pulsed electric fields. Trends in Food Science & Technology. 2002;13(6–7):195-204.

49. Cohen de Lara E. Electric field effect on molecules: Relation between the orientation of the molecule with respect to the field and the vibrational frequency shift observed in IR spectra of molecules adsorbed in zeolites. Physical Chemistry Chemical Physics. 1999;1(4):501-5.

50. Harada A, Kataoka K. Switching by Pulse Electric Field of the Elevated Enzymatic Reaction in the Core of Polyion Complex Micelles. J Am Chem Soc. 2003;125(50):15306-7.

51. Lin Z-R, Zeng X-A, Yu S-J, Sun D-W. Enhancement of Ethanol–Acetic Acid Esterification Under Room Temperature and Non-catalytic Condition via Pulsed Electric Field Application. Food Bioprocess Technol. 2012;5(7):2637-45.

52. Liu Y, Oh K, Bai JG, Chang C-L, Yeo W, Chung J-H, et al. Manipulation of nanoparticles and biomolecules by electric field and surface tension. Computer Methods in Applied Mechanics and Engineering. 2008;197(25–28):2156-72.

53. Ma S, Wang Z-h. Pulsed electric field-assisted modification of pectin from sugar beet pulp. Carbohydrate Polymers. 2013;92(2):1700-4.

54. Ohshima T, Tamura T, Sato M. Influence of pulsed electric field on various enzyme activities. Journal of Electrostatics. 2007;65(3):156-61.

55. Porschke D. Effects of Electric Fields on Biopolymers. Annual Review of Physical Chemistry. 1985;36(1):159-78.

56. Puértolas E, López N, Condón S, Álvarez I, Raso J. Potential applications of PEF to improve red wine quality. Trends in Food Science & Technology. 2010;21(5):247-55.

57. Tsuji K, Müller SC, Hess B. Electric field induced conformational changes of bacteriorhodopsin in purple membrane films. Eur Biophys J. 1988;15(6):329-37.

58. Yeom HW, Zhang QH, Dunne CP. Inactivation of papain by pulsed electric fields in a continuous system. Food Chemistry. 1999;67(1):53-9.

59. Zhao W, Yang R, Zhang HQ. Recent advances in the action of pulsed electric fields on enzymes and food component proteins. Trends in Food Science & Technology. 2012;27(2):83-96.

60. Zhong K, Hu X, Zhao G, Chen F, Liao X. Inactivation and conformational change of horseradish peroxidase induced by pulsed electric field. Food Chemistry. 2005;92(3):473-9.

61. Zimmermann RM, Cox EC. DNA stretching on functionalized gold surfaces. Nucleic Acids Research. 1994;22(3):492-7.

62. El‐Aila HJY. Effect of Triton‐X‐100 Solvent in the Micellar Catalysis of the Aquation of Tris(2‐nitroso‐1‐naphtholate) Ferrate (II). Journal of Dispersion Science and Technology. 2007;28(8):1201-4.

63. Fujii S, Isojima T, Sasaki N, Hamano K. Dynamic light scattering of an ionic SDS micellar solution under an AC electric field. Colloid Polym Sci. 2001;279(3):252-8.

64. Goodrich VE, Connor E, Wang S, Yang J, Zhao J, Zhu Y. AC-electrokinetic manipulation and controlled encapsulate release of surfactant based micelles. Soft Matter. 2013;9(20):5052-60.

65. Sonin AA, Kim M-G, Lee K-H, Kim J-Y, Jeong H-D, Kim M-W. Electric Field–Induced Ordering of the Worm-Like Micelles: Application to the Low-Dielectric-Constant Materials. Molecular Crystals and Liquid Crystals. 2006;452(1):27-36.

66. Streletzky K, Phillies GDJ. Temperature Dependence of Triton X-100 Micelle Size and Hydration. Langmuir. 1995;11(1):42-7.

67. Vijayan K, Geng Y, Discher D. Electric Field Manipulation of Charged Copolymer Worm Micelles†. The Journal of Physical Chemistry B. 2005;110(8):3831-4.

68. Clarke JM, Gillings MR, Altavilla N, Beattie AJ. Potential problems with fluorescein diacetate assays of cell viability when testing natural products for antimicrobial activity. Journal of Microbiological Methods. 2001;46(3):261-7.

69. Schnürer J, Rosswall T. Fluorescein Diacetate Hydrolysis as a Measure of Total Microbial Activity in Soil and Litter. Applied and Environmental Microbiology. 1982;43(6):1256-61.

70. Alarcón-Gutiérrez E, Floch C, Ruaudel F, Criquet S. Non-enzymatic hydrolysis of fluorescein diacetate (FDA) in a Mediterranean oak (Quercus ilex L.) litter. European Journal of Soil Science. 2008;59(2):139-46.

71. Bartczak D, Kanaras AG. Preparation of Peptide-Functionalized Gold Nanoparticles Using One Pot EDC/Sulfo-NHS Coupling. Langmuir. 2011;27(16):10119-23.

72. Haiss W, Thanh NTK, Aveyard J, Fernig DG. Determination of Size and Concentration of Gold Nanoparticles from UV−Vis Spectra. Analytical Chemistry. 2007;79(11):4215-21.

73. Kumar A, Ma H, Zhang X, Huang K, Jin S, Liu J, et al. Gold nanoparticles functionalized with therapeutic and targeted peptides for cancer treatment. Biomaterials. 2012;33(4):1180-9.

74. Martin MN, Basham JI, Chando P, Eah S-K. Charged Gold Nanoparticles in Non-Polar Solvents: 10-min Synthesis and 2D Self-Assembly. Langmuir. 2010;26(10):7410-7.

75. Liu Y, Shipton MK, Ryan J, Kaufman ED, Franzen S, Feldheim DL. Synthesis, Stability, and Cellular Internalization of Gold Nanoparticles Containing Mixed Peptide−Poly(ethylene glycol) Monolayers. Analytical Chemistry. 2007;79(6):2221-9.

76. Lindqvist Y, Huang W, Schneider G, Shanklin J. Crystal structure of delta9 stearoyl-acyl carrier protein desaturase from castor seed and its relationship to other di-iron proteins. The EMBO Journal. 1996;15(16):4081-92.

77. Shanklin J, Achim C, Schmidt H, Fox BG, Münck E. Mössbauer studies of alkane ω-hydroxylase: Evidence for a diiron cluster in an integral-membrane enzyme. Proceedings of the National Academy of Sciences of the United States of America. 1997;94(7):2981-6.